

General protocols for the efficient distillation of indistinguishable photons

Jason Saied,^{1,*} Jeffrey Marshall,^{1,2,†} Namit Anand,^{1,3} and Eleanor G. Rieffel¹

¹*QuAIL, NASA Ames Research Center, Moffett Field, CA 94035, USA*

²*USRA Research Institute for Advanced Computer Science, Mountain View, CA 94043, USA*

³*KBR, Inc., 601 Jefferson St., Houston, TX 77002, USA*

Highly pure and indistinguishable photons are a prerequisite for use in quantum information processing. We introduce protocols for the distillation of indistinguishable photons that offer a significant improvement over previous work, reducing distinguishability error rates by a factor of n , with resource requirements scaling linearly in n . We present the protocols, based on the discrete Fourier transform and Hadamard (Sylvester) matrices, then give both analytical and numerical results regarding their performance. We observe that the same symmetry properties governing suppression laws are instrumental in understanding the behavior of these distillation protocols. We also prove, adapting a result from the Hadamard case, that for the n -photon discrete Fourier transform with n a prime power, the suppression laws are exactly characterized by the well-known Zero Transmission Law based on permutation symmetry.

CONTENTS

I. Introduction	2
II. Preliminaries	4
A. Linear optics	4
B. Models for distinguishability	8
III. Main results	10
A. Distillation protocols	10
B. Heralding rates	12
C. Comparison of resource costs	15
D. Symmetries and conjectures	17
E. Numerics	20
F. Incorporation of photon loss	23
IV. Discussion	26
V. Acknowledgements	27
References	28
A. Symmetry	30

* jason.saied@nasa.gov

† jmarshall@usra.edu

1. General case	30
2. Fourier case	32
3. Hadamard case	34
B. Detailed calculations	35
1. Heralding rate	35
2. Error rate	39
3. First order approximations	41
C. Haar random case	42
D. Numerics	46

I. INTRODUCTION

Highly pure and indistinguishable photons are a prerequisite for use in quantum information processing. The effect of distinguishability has been famously demonstrated by the Hong-Ou-Mandel (HOM) experiment, which shows fundamentally different statistics in the cases when photons are identical or not. The HOM effect (and its generalizations) is a crucial ingredient for realizing linear optical quantum computation (QC) [1], where the interference between identical photons can be used to create entanglement over computational degrees of freedom (aided by post-selective measurements). For example, fusion measurements can be used to create large cluster states out of primitive entangled states, such as Bell states or small Greenberger-Horne-Zeilinger (GHZ) states [2]. These states can then be used to realize fault-tolerant quantum computation, in paradigms such as fusion-based QC [3]. However, the presence of distinguishability will generally result in less entanglement generated over the computational degrees of freedom [4, 5], meaning their computational ‘resource’ is reduced. In fact, the degree of distinguishability has been shown to reduce the classical computational complexity (and thus potential quantum advantage) of boson sampling [6]. Distinguishability between photons can also be unheralded (since the correct number of photons are eventually detected), making such errors potentially harder to deal with in linear optical QC than photon loss, the dominant source of noise in linear optics, which is generally heralded.

The conventional approach to achieving highly pure photons relies upon spectral filtering. While spectral filtering can produce very uniform photons, it has drawbacks. First, such methods are typically unheralded, meaning if a single photon impinges upon a filter, it is unknown if it exited the filter. Second, as the target fidelity is increased, the probability a photon passes the filter decreases [7]. To overcome these issues, in 2017 a fully linear optical scheme (with Fock basis measurements) to distill indistinguishable photons from partly distinguishable ones was presented [4], which was subsequently improved upon in Ref. [8]. An experimental demonstration of the distillation scheme of Ref. [4] was recently given in Ref. [9].

Current experiments typically measure the degree of photon-photon distinguishability in linear optics via a HOM dip which counts coincidence events, allowing one to compute the *visibility* $V = \text{Tr}[\rho_a \rho_b]$, where e.g. ‘*a*’, ‘*b*’ label two different photon sources. Values for the visibility vary

quite a bit, depending on the type of single photon source used, photon encoding, spectral filtering, etc., with an approximate range found in the literature to be $V \in [0.74, 0.97]$ [10–15]. In this work we characterize the error via a parameter $\epsilon \approx 1 - \sqrt{V}$ (discussed in Sect. II B), which for reference gives ϵ approximately in the range $[0.02, 0.15]$, based on the quoted visibility values.

The general idea of these distillation protocols is shown in Fig. 1, whereby n (noisy) single photons are evolved under a linear optical unitary, with post-selection performed by photon-number-resolving detectors (PNRD). It can be shown that by carefully performing the post-selection based on the interference generated by the unitary evolution, one can guarantee that the output photons will have a higher expected overlap with the target state. In this work we generalize the state-of-the-art 3 and 4 photon protocols of Ref. [8] to allow the scheme to work with any number n of photons (as in Fig. 1) and achieve more efficient distillation.

These generalized protocols depend on an $n \times n$ unitary matrix U . We consider protocols with U coming from the discrete Fourier transform F_n (for $n \geq 3$) and Hadamard matrices $H_n = H^{\otimes r}$, where H is the 2×2 Hadamard matrix and $n = 2^r$. The 3 and 4 photon protocols of [8] correspond to the cases $U = F_3$ and $U = H_4$ respectively. We prove (see Theorem III.2) that for input photons with distinguishability error rate ϵ (defined in Section II B below), the protocol heralds the output of single photons with distinguishability error rate $e_n(\epsilon) \approx \epsilon/n$. In particular, large enough values of n lead to arbitrary reduction of the distinguishability error rate.

As with the earlier works [4, 8], these protocols are non-deterministic with some *heralding rate* $h_n(\epsilon) < 1$, the probability of heralding the output of a distilled single photon. Large heralding rates are desirable in order to minimize overhead. In Theorem III.3, we give a formula for the heralding rate $h_n(\epsilon)$ up to first order in ϵ , depending only on the heralding rate in the error-free case, $h_n(0)$. In Theorem III.4 and the following discussion, we give a formula for $h_n(0)$ in terms of hypergeometric functions and observe that it quickly approaches $1/4$, with $h_n(0) - \frac{1}{4} \sim \frac{1}{16n}$. In particular, for small error rates ϵ (and $n \geq 4$), the n -photon distillation protocol succeeds with probability near $1/4$, and therefore we expect to use $n/4$ input photons to obtain an output photon with reduced error rate approximately ϵ/n . This is a significant improvement over the protocol of Sparrow and Birchall [4], which requires exponentially many photons to achieve the same reduced error rate ϵ/n [8]. Versions of the protocols of [4] and [8] involving active feed-forward during distillation may be used to obtain similar error rates with cubic or quadratic resources respectively; this is in contrast to our protocols, which require only linearly scaling resources *without* active feed-forward during distillation. In Section III C, we return to the comparison of resource requirements and error rates handled by the protocols in [4, 8] and the present protocols. Generally, we see that for small ϵ , the new protocols achieve comparable reduction in error at lower cost. However, each protocol has a *threshold* value of ϵ above which it fails to reduce the error rate; as n increases, this threshold decreases. Further, even below threshold, it can be advantageous to use smaller n protocols initially, feeding those into larger n protocols at the next stage. We discuss the design of such iterated distillation schemes.

For larger values of ϵ , the first-order approximations of $h_n(\epsilon)$ discussed above no longer suffice. In Section III D we conjecture a lower bound on $h_n(\epsilon)$ as a function of ϵ . This lower bound may be used to give explicit guarantees on the heralding rate for large n , as long as ϵ is sufficiently small relative

to n . For example, if $\epsilon \leq 1/n$, we conjecture that the n -photon protocol’s heralding rate is bounded below by $\frac{1}{4e} \approx 0.092$. These conjectures are supported by numerical evidence and are motivated by certain symmetry properties of the distillation protocols, discussed in Sect. III D. These symmetry properties are related to the suppression laws of [16–18] that underlie our main results and motivate the use of the Fourier and Hadamard unitaries. These suppression laws have also been applied to the related problem of verifying boson sampling devices [19, 20]. For the Hadamard case, the suppression is entirely governed by certain parity-preservation conditions determined by the symmetries [17, 18]. For the Fourier transform, the corresponding *Zero Transmission Law* (ZTL) was only known to determine some of the suppression, with cases (the smallest being F_6) in which there are more suppressed patterns than dictated by the ZTL [21]. In Theorem III.9, we prove that if n is a prime power, then the suppressed patterns are exactly determined by the ZTL.

In Sect. III E, we give some numerics of interest. We provide detailed analysis of the case $n = 8$ as a representative example. This is the smallest new protocol with n a power of 2, which means that we may consider both Fourier and Hadamard distillation protocols on the same number of photons and compare their performance. We also study the following problem: given an approximately known input error rate ϵ , which distillation protocol gives the greatest reduction in error if we are free to choose the value of n ? This problem is numerically answered for $n \leq 16$ in Figures 6 and 7. We observe several interesting trends in these results, related to the symmetry properties of Section III D. In particular, the optimal protocols seem to be Fourier transform protocols in which there are *more* suppressed patterns than explained by the ZTL (i.e., by Theorem III.9, with n not a prime power).

In Sect. III F, we consider the effect of photon loss on our protocols. Since photon loss will be detected by a distillation protocol with high probability (especially for large n), we are most concerned with the effect on the heralding rates (and thus the resource requirements). We give numerics and prove lower bounds on the lossy heralding rates as a function of $h_n(\epsilon)$, thus obtaining upper bounds on the required resources. In the $\epsilon = 0$ limit, the lower bound is exactly attained.

We further demonstrate in App. C that the ability to distill photons is in fact typical, as shown by a randomized scheme based on Haar sampled unitaries. However, these versions are significantly less resource efficient (requiring a far greater number of photons) compared to those based on the Fourier or Hadamard matrices, due to a greater degree of constructive interference as a result of symmetries present in these matrices (as discussed in Sect. III D).

While readers familiar with linear optics should be able to skip most of the preliminaries in Section II, we recommend reviewing the notation used in Section II B, especially the error models and (II.15).

II. PRELIMINARIES

A. Linear optics

In what follows, we will consider the space of n photons (not necessarily indistinguishable) in m (external) modes. We begin with the *first quantization*, following the notation of [22]. In

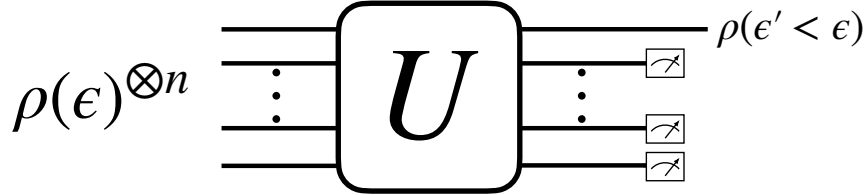


FIG. 1: Cartoon of n -photon distillation scheme, where n photons are injected into a linear optical unitary U . PNRDs are used to post-select on certain $n - 1$ photon outcomes, resulting in a single photon out (in the absence of losses/dark counts etc.). It is possible to engineer the unitary and post-selection criteria so that the output single-photon error is reduced.

this framework, each photon has state space $\mathcal{H} = \mathcal{H}_{\text{ext}} \otimes \mathcal{H}_{\text{int}}$, where \mathcal{H}_{ext} corresponds to the “external” modes—those manipulated by the experiment—and \mathcal{H}_{int} corresponds to the “internal” modes—those not manipulated by the experiment. We identify $\mathcal{H}_{\text{ext}} = \mathbb{C}^m$ with basis $|0\rangle, \dots, |m - 1\rangle$, where $|k\rangle$ describes a photon in mode k . The state space corresponding to n such photons is

$$\mathcal{H}^{\otimes n} = \mathcal{H}_{\text{ext}}^{\otimes n} \otimes \mathcal{H}_{\text{int}}^{\otimes n}. \quad (\text{II.1})$$

Given a $|\psi\rangle \in \mathcal{H}^{\otimes n}$, it has a corresponding *external density matrix* in $\mathcal{H}_{\text{ext}}^{\otimes n}$ obtained by taking the partial trace over $\mathcal{H}_{\text{int}}^{\otimes n}$. For experiments involving only linear optics on the external modes, the behavior of the state is fully characterized by its external density matrix [22]. For our purposes, however, we will often need to consider both the external and internal degrees of freedom.

The standard basis for $\mathcal{H}_{\text{ext}}^{\otimes n}$ in the first quantization picture is $|m_1, \dots, m_n\rangle = |m_1\rangle \otimes \dots \otimes |m_n\rangle$, where the i th photon is in mode $m_i \in \{0, \dots, m - 1\}$. When it is necessary to clarify that a state is using first quantization notation, we will instead write $|m_1, \dots, m_n\rangle_{1Q}$.

In this work, we will consider many different representations of permutation groups on $\mathcal{H}^{\otimes n}$ and the related subspaces. In the *photon permutation representation*, the symmetric group S_n acts on $\mathcal{H}^{\otimes n}$ by permuting the tensor factors, thus permuting the particles. In [22], it is assumed that photonic states are symmetric with respect to permutation of particles. However, as discussed below, in the presence of distinguishability we often find it mathematically convenient to consider more general states in $\mathcal{H}^{\otimes n}$.

The group $U_{n,m}$ of *linear optical unitaries* is the group of unitary operators on $\mathcal{H}^{\otimes n} = \mathcal{H}_{\text{ext}}^{\otimes n} \otimes \mathcal{H}_{\text{int}}^{\otimes n}$ of the form $U^{\otimes n} \otimes I^{\otimes n}$, where $U \in U(m)$ is an m -mode unitary operator on \mathcal{H}_{ext} . In particular, linear optical unitaries operate only on the external degrees of freedom and are symmetric with respect to permutation of photons. We will often write \hat{U} to denote the linear optical unitary corresponding to $U \in U(m)$; when the context is clear, we often simply write U . We also extend the notation to arbitrary operators T on \mathcal{H}_{ext} (not necessarily unitary), writing \hat{T} for the operator $T^{\otimes n} \otimes I^{\otimes n}$ on $\mathcal{H}^{\otimes n} = \mathcal{H}_{\text{ext}}^{\otimes n} \otimes \mathcal{H}_{\text{int}}^{\otimes n}$.

We will also use the *second quantization* representation of photonic states. We begin with the case in which only external degrees of freedom are considered. In this setting, we use the *Fock*

basis states $|n_0, \dots, n_{m-1}\rangle = |n_0, \dots, n_{m-1}\rangle_{2Q}$, which describe an m -mode state with n_0 photons in mode 0, n_1 photons in mode 1, and so on. For any mode i , we consider the *creation operator* acting on that mode,

$$a_i^\dagger = \sum_{n \geq 0} \sqrt{n+1} |n+1\rangle \langle n|_i. \quad (\text{II.2})$$

We also have $a_i = (a_i^\dagger)^\dagger$, the corresponding annihilation operator. Representing the *vacuum* state by $|\vec{0}\rangle$, we may express all Fock basis states (up to normalization) by applying appropriate creation operators:

$$|n_0, \dots, n_{m-1}\rangle_{2Q} = \frac{1}{\sqrt{n_0! n_1! \dots n_{m-1}!}} (a_0^\dagger)^{n_0} \dots (a_{m-1}^\dagger)^{n_{m-1}} |\vec{0}\rangle. \quad (\text{II.3})$$

Linear optical unitary evolution in the second quantization is characterized by the same $U \in U(m)$ matrix mentioned above, which independently evolves each creation operator: $a_j^\dagger \rightarrow \sum_{i=0}^{m-1} U_{ij} a_i^\dagger$. Note that the Fock basis states are symmetric with respect to permutation of photons: for example,

$$|1, 1\rangle_{2Q} = a_0^\dagger a_1^\dagger |\vec{0}\rangle = \frac{1}{\sqrt{2}} (|0, 1\rangle_{1Q} + |1, 0\rangle_{1Q}). \quad (\text{II.4})$$

Thus the Fock basis is a basis for the *symmetric subspace* of $\mathcal{H}_{\text{ext}}^{\otimes n}$.

Remark II.1. We may convert between first and second quantization as follows. We let F be the symmetrization map from $\mathcal{H}_{\text{ext}}^{\otimes n}$ to its symmetric subspace, with (for example)

$$F(|0, 1\rangle_{1Q}) = \frac{1}{\sqrt{2}} (|0, 1\rangle_{1Q} + |1, 0\rangle_{1Q}) = |1, 1\rangle_{2Q}. \quad (\text{II.5})$$

In particular, we have $F(|m_0, \dots, m_{n-1}\rangle_{1Q}) = |n_0, \dots, n_{m-1}\rangle_{2Q}$, where n_i is the number of photons in mode i (the number of indices j with $m_j = i$). The map F is not invertible, but given $|n_0, \dots, n_{m-1}\rangle_{2Q}$, there is a unique weakly increasing $|m_0, \dots, m_{n-1}\rangle_{1Q}$ with $F(|m_0, \dots, m_{n-1}\rangle_{1Q}) = |n_0, \dots, n_{m-1}\rangle_{2Q}$.

When there are internal degrees of freedom under consideration, we use the notation $a_i^\dagger[\xi_j]$ to indicate the creation of a particle with internal state $|\xi_j\rangle$ in external mode i . For a fixed orthonormal basis $\{|\xi_0\rangle, |\xi_1\rangle, \dots\}$ of \mathcal{H}_{int} , we will consider (normalized) vectors of the form

$$a_{m_0}^\dagger[\xi_{i_0}] \dots a_{m_{n-1}}^\dagger[\xi_{i_{n-1}}] |\vec{0}\rangle. \quad (\text{II.6})$$

These states are symmetric under permutation of photons, as the notation $a_k^\dagger[\xi_{i_j}]$ only indicates the mode and internal state, not the particular photon (tensor factor in $\mathcal{H}^{\otimes n}$). This is in alignment with [22]. We also introduce the *desymmetrized Fock states*, (non-bosonic) states with only the “necessary” symmetry determined by a fixed internal state $|\xi_{i_0}, \dots, \xi_{i_{n-1}}\rangle$, as follows. The external part is obtained by starting with some state $|m_0, \dots, m_{n-1}\rangle_{1Q}$ and, for each $j \geq 0$, symmetrizing

all photons k with $i_k = j$. For example, we consider

$$\frac{1}{\sqrt{2}} \left(|0, 1\rangle_{1Q} + |1, 0\rangle_{1Q} \right) \otimes |2\rangle_{1Q} \otimes |\xi_0, \xi_0, \xi_2\rangle. \quad (\text{II.7})$$

This state is symmetric with respect to permutations of photons 0 and 1, since those photons have the same internal state ξ_0 ; there is no symmetry with the second photon, since it has internal state $|\xi_2\rangle$ orthogonal to $|\xi_0\rangle$. The desymmetrized Fock states are motivated in Remark II.2. We will generally be interested in states that are linear combinations of desymmetrized Fock states. We note that the space of all such states is preserved under linear optics.

We will consider two main types of measurements. The first is *photon number resolving detection* (PNRD), formalizing the notion of a measurement that counts the number of photons in each mode. (We may also perform PNRD on a subset of modes in the obvious way.) This is a projective measurement on $\mathcal{H}_{\text{ext}}^{\otimes n}$, projecting onto the subspaces V_{n_1, \dots, n_m} where

$$V_{n_0, \dots, n_{m-1}} = \text{span}\{|m_0, \dots, m_{n-1}\rangle_{1Q} : F(|m_0, \dots, m_{n-1}\rangle_{1Q}) = |n_0, \dots, n_{m-1}\rangle_{2Q}\} \quad (\text{II.8})$$

(recalling the map F of Remark II.1). This is just the space spanned by all states with n_0 photons in mode 0, n_1 photons in mode 1, and so on. We call (n_0, \dots, n_{m-1}) the obtained *measurement pattern*. For symmetric states in $\mathcal{H}_{\text{ext}}^{\otimes n}$, PNRD is simply projection onto the Fock basis; the above version allows for nonsymmetric states and internal degrees of freedom. Note that the internal degrees of freedom may be traced out for PNRD. Before giving the other type of measurement, we briefly discuss the desymmetrized Fock states in more detail.

Remark II.2. *We consider the states (II.6), a natural basis for the space of symmetric states in $\mathcal{H}^{\otimes n}$. We may write such a state $|\psi\rangle$ as a linear combination of (non-symmetric) orthogonal desymmetrized Fock states $|\psi_\pi\rangle$, each with an internal state of the form $|\xi_{\pi(i_1)}, \dots, \xi_{\pi(i_r)}\rangle$, where π is a nontrivial permutation of (i_1, \dots, i_r) . Since linear optical unitaries only resolve and manipulate the external degrees of freedom, terms with orthogonal internal states cannot interfere. Thus, $|\psi\rangle$ behaves equivalently to the mixed state corresponding to an even mixture of the orthogonal terms $|\psi_\pi\rangle$. Comparing two such terms $|\psi_\pi\rangle, |\psi_{\pi'}\rangle$, we see that each involves the same number of photons in each external mode, and within each external mode there are the same number of photons with internal state $|\xi_0\rangle, |\xi_1\rangle$, etc. The only difference is the order of the tensor factors. This information is not taken into account by linear optical unitaries or PNRD. Thus, we often find it convenient to “de-symmetrize” a state of the form (II.6), replacing it with a desymmetrized Fock state. For example, we may represent $a_0^\dagger[\xi_0]a_1^\dagger[\xi_0]a_2^\dagger[\xi_2]|\vec{0}\rangle$ by the desymmetrized Fock state given in (II.7) above.*

For certain calculations, we will be interested in measuring the internal modes as well. We note, however, that this will only be used mathematically, to calculate output error rates of distillation protocols; the protocols themselves do not require any measurements beyond PNRD. Specifically, *internal-external measurement* is a refinement of PNRD in which we measure the number of photons with each possible internal state $|\xi_i\rangle$ in each mode. Mathematically, this corresponds to projecting onto the subspaces spanned by all permutations of some fixed desymmetrized Fock state.

Finally, we define perfect indistinguishability of photons, following [22]. Let ρ be a density matrix, and let ρ_{ext} be the corresponding external state, obtained by tracing out the internal Hilbert space. Let $P^{(n)}$ be the symmetrizer on \mathcal{H}_{ext} , projecting to states that are invariant under permutation of photons. Then ρ is *perfectly indistinguishable* if $P^{(n)}\rho_{\text{ext}} = \rho_{\text{ext}}$. The main examples in this paper correspond to states $\rho = |\psi\rangle\langle\psi|$, where $|\psi\rangle = a_{m_0}^\dagger[\xi_0] \cdots a_{m_{n-1}}^\dagger[\xi_0]|\vec{0}\rangle$. More generally, any state $|\psi\rangle$ that can be expressed as a pure tensor $|\psi_{\text{ext}}\rangle \otimes |\psi_{\text{int}}\rangle$, with $|\psi_{\text{ext}}\rangle$ and $|\psi_{\text{int}}\rangle$ symmetric under permutation of photons, is perfectly indistinguishable. We discuss a nontrivial such example in Appendix B 3. On the other hand, any state of the form (II.6) involving two distinct (orthogonal) internal states $|\xi_i\rangle, |\xi_j\rangle$ is *not* perfectly indistinguishable.

B. Models for distinguishability

Following [8, 23, 24], we will consider variants of the *random source* (RS) model for photon distinguishability, in which photon sources independently produce photons with average internal state $\rho = \sum_{j \geq 0} p_j |\xi_j\rangle\langle\xi_j|$, where the $|\xi_j\rangle$ range over an orthonormal basis for \mathcal{H}_{int} . We fix this basis $\{|\xi_0\rangle, |\xi_1\rangle, \dots\}$ for \mathcal{H}_{int} going forward. Note that this model is equivalent, under the assumption that the internal degrees of freedom cannot be resolved or manipulated by the experiment, to a pure state description $\sum_j e^{i\phi_j} \sqrt{p_j} |\xi_j\rangle$ [4, 24]. Without loss of generality, we assume that p_0 is the dominant eigenvalue and write $\epsilon = 1 - p_0 = \sum_{j \geq 1} p_j$, so that

$$\rho = \rho(\epsilon) = (1 - \epsilon) |\xi_0\rangle\langle\xi_0| + \epsilon \sum_{j \geq 1} p'_j |\xi_j\rangle\langle\xi_j| \quad (\text{II.9})$$

in the RS model, with $p'_j = p_j/\epsilon$. We write $\rho = \rho(\epsilon)$ to emphasize the dependence on the parameter ϵ (suppressing the p_i from the notation). We view the state as a probabilistic mixture: with large probability $1 - \epsilon$ we obtain the “ideal” state $|\xi_0\rangle$, and with small probability ϵ we obtain one of the “distinguishable” error states $|\xi_j\rangle$, orthogonal to $|\xi_0\rangle$. In terms of creation operators, we may represent $\rho(\epsilon)$ by the appropriate probabilistic mixture of the creation operators $a^\dagger[\xi_j]$.

In this work, we often restrict our attention to the *uniform RS* (URS) model, in which we take $p'_1 = p'_2 = \dots = p'_R = 1/R$ and $p_j = 0$ for $j > R$, so that

$$\rho(\epsilon) = (1 - \epsilon) |\xi_0\rangle\langle\xi_0| + \frac{\epsilon}{R} \sum_{j=1}^R |\xi_j\rangle\langle\xi_j|. \quad (\text{II.10})$$

For ease of exposition and simulation, we will often consider two extreme cases that are useful for restricting the possible internal states. First, we have the *Same Bad Bits* (SBB) model [24], where we take $R = 1$ in the URS model, so that each photon has average internal state

$$\rho(\epsilon) = (1 - \epsilon) |\xi_0\rangle\langle\xi_0| + \epsilon |\xi_1\rangle\langle\xi_1|. \quad (\text{II.11})$$

This model captures a situation with systematic errors in which photons are prone to exhibit the same type of distinguishability error. This may be viewed as the special case in which the internal

state space \mathcal{H}_{int} is 2-dimensional. On the other hand, we consider the Orthogonal Bad Bits (OBB) model, where the i th photon has internal state

$$\rho_i(\epsilon) = (1 - \epsilon) |\xi_0\rangle\langle\xi_0| + \epsilon |\xi_{i+1}\rangle\langle\xi_{i+1}|. \quad (\text{II.12})$$

Recall that $\langle\xi_i|\xi_j\rangle = \delta_{ij}$. As discussed in [23], this corresponds to the limit of the URS model as $R \rightarrow \infty$. This model captures a situation in which error states are uniformly random with many degrees of freedom, so that it is vanishingly unlikely for the same error to occur twice in the same experiment. Since the OBB and SBB models may be viewed as opposite extremes of the URS model, we choose them as a particular focus for numerical simulation and examples.

Finally, we compare our parameter ϵ to the *visibility*. In the URS model, one can compute the visibility between two states drawn from the distribution as $V = \text{Tr}[\rho(\epsilon)^2] = (1 - \epsilon)^2 + \epsilon^2/R$. For the OBB limit, this gives visibility $V = (1 - \epsilon)^2$. In any case we have $V = 1 - 2\epsilon + O(\epsilon^2)$, so when V is large there is little difference between the corresponding values of ϵ in different error models. Using the above, visibility $V \geq 0.74$ (a rough lower bound on experimental visibility values in some recent literature [10–15]) approximately translates to $\epsilon \leq 0.15$. We are therefore primarily interested in effective distillation protocols for these relatively small values of ϵ .

1. Initial states

We briefly return to the general RS model. We will take $m = n$, considering experiments in which n photons are injected into n different (external) modes of an interferometer, with the photon in mode i having internal state $\rho_i(\epsilon)$. When $\epsilon = 0$ and internal degrees of freedom are neglected, this corresponds to the idealized Fock state $|1, \dots, 1\rangle_{2Q}$. In general, we call the initial state $\rho^{(n)} = \rho^{(n)}(\epsilon)$. Note that in this setting, we may label photon i as the photon initialized in input mode i , giving an unambiguous, natural correspondence between terms of the form (II.6) and desymmetrized Fock states. (Recall Remark II.2.) We may decompose $\rho^{(n)}$ as follows:

$$\rho^{(n)} = \sum_{j_0, \dots, j_{n-1}} (p_{j_0} \cdots p_{j_{n-1}}) a_0^\dagger[\xi_{j_0}] \cdots a_{n-1}^\dagger[\xi_{j_{n-1}}] |\vec{0}\rangle\langle\vec{0}| a_0[\xi_{j_0}] \cdots a_{n-1}[\xi_{j_{n-1}}]. \quad (\text{II.13})$$

This is a probabilistic mixture of many terms; fixing the labeling of the photons as above, each corresponds to a desymmetrized Fock state with internal state of the form $|\xi_{j_1}, \dots, \xi_{j_n}\rangle$. By abuse of notation, we write

$$a_0^\dagger[\xi_{j_0}] \cdots a_{n-1}^\dagger[\xi_{j_{n-1}}] |\vec{0}\rangle = |1, \dots, 1\rangle_{2Q} \otimes |\xi_{j_0}, \dots, \xi_{j_{n-1}}\rangle. \quad (\text{II.14})$$

Note that in general, the left-hand side is not actually a pure tensor. For example, $a_0^\dagger[\xi_0] a_1^\dagger[\xi_1] |\vec{0}\rangle = |0, 1\rangle_{1Q} \otimes |\xi_0, \xi_1\rangle + |1, 0\rangle_{1Q} \otimes |\xi_1, \xi_0\rangle$. The corresponding desymmetrized Fock state is written $|1, 1\rangle_{2Q} \otimes |\xi_0, \xi_1\rangle$ and involves only one of the two terms, $|0, 1\rangle_{1Q} \otimes |\xi_0, \xi_1\rangle$ by our convention. This state is *not* symmetric under permutation of photons, but behaves equivalently to the full state under linear optics and PNRD.

We say that a state (II.14) has k *distinguishability errors*, where k is the number of indices i with $j_i \neq 0$. We will often consider small values of ϵ , so that the expression is dominated by the terms that are first order or less in ϵ ; in other words, those with 0 or 1 distinguishability errors. We note that, for any RS model, the weight of the terms with exactly 1 distinguishability error is $n(1 - \epsilon)^{n-1} \sum_{j \geq 1} p_j = n\epsilon(1 - \epsilon)^{n-1}$. For the calculations of interest, we will see that these first-order terms exhibit essentially the same behavior regardless of the particular model.

In the URS model (or its OBB limit), we write the input state as

$$\rho^{(n)}(\epsilon) = \sum_{k=0}^n \binom{n}{k} \epsilon^k (1 - \epsilon)^{n-k} \Phi_k, \quad (\text{II.15})$$

where Φ_k is the mixed state involving all terms with k distinguishability errors, normalized to have $\text{Tr}(\Phi_k) = 1$. Going forward, we will exclusively discuss the URS framework, but the results involving only terms with 0 or 1 distinguishability errors, such as Theorems III.2, III.3, III.4, III.8, III.10 in fact hold for any RS model.

III. MAIN RESULTS

A. Distillation protocols

In this work, we will consider *distillation protocols* generalizing the work of [8], described in Protocol III.1 and illustrated in Figure 1. Unless stated otherwise, we assume that the only errors are distinguishability errors, and we model distinguishability with the URS error model (or the OBB limit) with error rate ϵ . (Photon loss will be addressed in Section III F.)

Consider an $n \times n$ matrix U . Define the set of *ideal patterns* corresponding to U to be the set of all (n_0, \dots, n_{n-1}) such that

$$n_0 = 1 \text{ and } \langle n_0, \dots, n_{n-1} | \hat{U} | 1, \dots, 1 \rangle \neq 0, \quad (\text{III.1})$$

where both states are Fock basis states (with no internal degrees of freedom).

Protocol III.1. *Given a number n of modes and an $n \times n$ unitary matrix U (corresponding to a linear optical unitary), we describe the corresponding n -photon distillation protocol.*

1. *Input a state σ of n photons in n distinct modes. We will typically consider $\sigma = \rho^{(n)}(\epsilon)$.*
2. *Apply \hat{U} , mapping $\sigma \mapsto \mu = \hat{U}\sigma\hat{U}^\dagger$.*
3. *Perform PNRD on the final $n-1$ modes of μ , obtaining a measurement pattern (n_1, \dots, n_{n-1}) with n_i being the number of photons found in mode i . Label mode 0, the unmeasured mode, as the output mode; we call the single-mode post-measurement state the output state. Letting $n_0 = n - \sum_{j \geq 1} n_j$, the output state has n_0 photons. We call (n_0, \dots, n_{n-1}) the corresponding completed measurement pattern.*

4. Post-select for ideal patterns, as defined in (III.1). In other words, if the pattern is not ideal, the photon is rejected.

The purpose of the distillation protocol is to herald the output of single photons with reduced distinguishability error rate, enabling more efficient linear optical quantum computation. By post-selecting for patterns with $n_0 = 1$, we guarantee that the output state has a single photon. (Assuming distinguishability is the only error.) By post-selecting for ideal patterns in particular, we *herald* the output of a single photon with (hopefully) a smaller rate of distinguishability error. This is simply an application of conditional probability: one needs to show that, given the knowledge that the completed measurement pattern is ideal, the output photon is more likely to be ideal.

Given such a distillation protocol with input state $\sigma = \rho^{(n)}(\epsilon)$, there will be two main metrics of interest, functions of the input error rate ϵ . First is the *heralding rate* $h_n(\epsilon)$, the probability of obtaining an ideal pattern during the measurement step. Second is the *output error rate* $e_n(\epsilon)$. If distinguishability is the only error, this is the probability that, given the heralding of an ideal pattern, the output photon has a “distinguishable” internal state $|\xi_i\rangle$, $i > 0$. (This is made rigorous via an internal-external measurement, as discussed in Section II A. We discuss the case in which there are loss errors in addition to distinguishability in Section III F.) For an arbitrary density matrix σ , we write $h_n(\sigma)$, $e_n(\sigma)$ to be the corresponding heralding and output error rates for the distillation protocol with input state σ .

We will be particularly interested in protocols using the quantum Fourier transform and Hadamard matrices. We briefly discuss these matrices and the corresponding ideal patterns now: for a more detailed analysis, we refer to Appendix A. We also compare to the case of Haar random matrices in Appendix C.

The Hadamard matrices under consideration are defined for $n = 2^r$ by $H_n = H^{\otimes r}$, where H is the standard 2×2 Hadamard matrix. (We note that this family is typically called the family of *Sylvester matrices*.) A recursive linear optical circuit for H_n is given in Figure 9. For H_n , we always take n to be a power of 2, even if not explicitly stated. The case $n = 4$ is equivalent to the 4-photon distillation protocol in the appendix of [8], where there is only one ideal pattern, $(1, 1, 1, 1)$. To describe the ideal patterns for H_n , we take a completed measurement pattern $p = (n_0, \dots, n_{n-1})$ and “convert to first quantization,” obtaining integers $0 \leq g_0 \leq g_1 \leq \dots \leq g_{n-1} \leq m - 1$ such that n_i is the number of indices j with $g_j = i$. For example, $p = (1, 2, 0, 1)$ corresponds to $g = (0, 1, 1, 3)$. With this notation, the ideal patterns for H_n are exactly those satisfying $n_0 = 1$ and $g_0 \oplus \dots \oplus g_{n-1} = 0$, where \oplus is binary XOR without carrying [17].

Letting $\omega = \exp(2\pi i/n)$, the n -mode Fourier transform matrix is given by

$$F_n = \frac{1}{\sqrt{n}}(\omega^{ij})_{0 \leq i, j \leq n-1}. \quad (\text{III.2})$$

The distillation protocol for F_3 is equivalent to the 3-photon protocol in the main text of [8], where there is only one ideal pattern, $(1, 1, 1)$. With the same “first quantization” notation as above, the ideal patterns for F_n satisfy the *Zero Transmission Law (ZTL)*, $g_0 + \dots + g_{n-1} \equiv 0 \pmod n$

[18, 21]. In Theorem III.9, we prove that whenever n is a prime power, then the ideal patterns are exactly characterized by the ZTL. For general n , however, the set of ideal patterns may be a proper subset of those satisfying this condition (and $n_0 = 1$). We further discuss these properties in Sections III D and Appendix A 2 below.

We have the following result for the Fourier and Hadamard distillation protocols.

Theorem III.2. *Consider an n -photon distillation protocol with unitary $U = F_n$ ($n \geq 3$) or H_n ($n = 2^r \geq 4$) and input state $\rho^{(n)}(\epsilon)$. The output error rate satisfies*

$$e_n(\epsilon) = \frac{\epsilon}{n} + O(\epsilon^2). \quad (\text{III.3})$$

This is proven in Appendix B 3. As a consequence of the theorem, we see that for sufficiently small ϵ , $e_n(\epsilon) \approx \epsilon/n$. Then, when ϵ is small enough, the protocols with larger n are better at reducing distinguishability errors. This is visible in Figure 2. However, we note that as ϵ grows, the protocols with large n tend to perform worse. In particular, each protocol has a *distillation threshold*, a value of ϵ after which it does not necessarily reduce the error rate. We numerically plot some representative threshold values in Figure 3; these values appear to decrease as n increases, likely approaching 0 in the limit $n \rightarrow \infty$. For practical values of n , however, the thresholds are reasonably large. For example, the 16-photon protocols improve the error rate as long as $\epsilon < 0.179$ (for OBB and SBB error models).

In order to understand the utility of a distillation protocol, we must also consider the heralding rate, which determines the resource cost. We investigate this problem in Section III B.

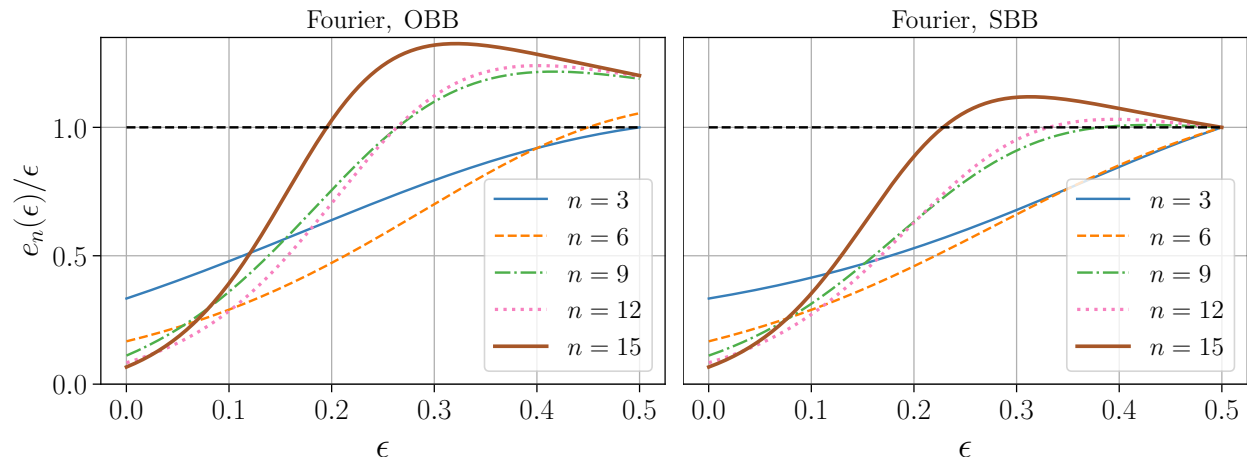


FIG. 2: Plot of the error rate reduction with OBB (left) and SBB (right) error models, for the Fourier distillation protocol. For $\epsilon \rightarrow 0$, $e_n(\epsilon)/\epsilon \rightarrow 1/n$. Distillation is successful at reducing the error rate when the curve is less than 1, marked by the horizontal dashed line. (Also see Fig. 3).

B. Heralding rates

For a distillation protocol with heralding probability $h_n(\epsilon)$, we expect to repeat it $1/h_n(\epsilon)$ times in order to successfully herald a distilled output photon. Since each iteration involves n photons,

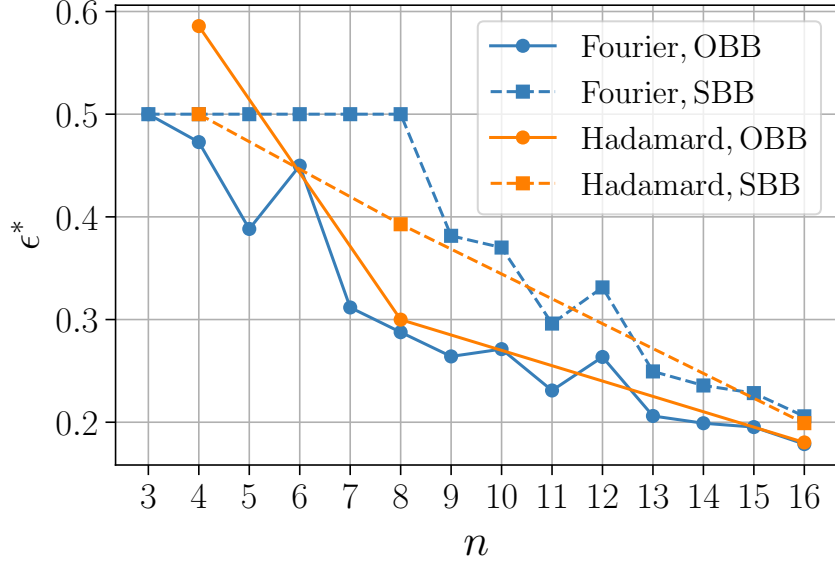


FIG. 3: Plot of the distillation thresholds, the smallest value $\epsilon^* > 0$ such that $e_n(\epsilon^*) = \epsilon^*$. In particular, distillation is advantageous for the given protocol, as long as the initial error ϵ satisfies $\epsilon < \epsilon^*$. We plot both SBB and OBB noise models, for Hadamard and Fourier matrices. Numerically we observe the Fourier OBB case to scale approximately as $\epsilon^* \sim 1/n^{0.61}$.

the expected number of photons required for a single distilled output photon is then $n/h_n(\epsilon)$. Thus, we are interested in estimating the heralding rate, and especially obtaining lower bounds, in order to obtain upper bounds on the required resources.

Recalling the decomposition (II.15) for $\rho^{(n)}(\epsilon)$, we have

$$h_n(\epsilon) = \sum_{k=0}^n \binom{n}{k} \epsilon^k (1-\epsilon)^{n-k} h_n(\Phi_k) \quad (\text{III.4})$$

$$= (1-\epsilon)^n h_n(\Phi_0) + n\epsilon(1-\epsilon)^{n-1} h_n(\Phi_1) + O(\epsilon^2) \quad (\text{III.5})$$

$$= h_n(\Phi_0) + \epsilon n(h_n(\Phi_1) - h_n(\Phi_0)) + O(\epsilon^2). \quad (\text{III.6})$$

Thus, for sufficiently small ϵ , the heralding rate is determined by $h_n(\Phi_0) = h_n(0)$ and $h_n(\Phi_1)$, corresponding to heralding rates for input states with 0 or 1 errors. We have:

Theorem III.3. Consider an n -photon distillation protocol with unitary $U = F_n$ ($n \geq 3$) or H_n ($n = 2^r \geq 4$) and input state $\rho^{(n)}(\epsilon)$.

1. We have $h_n(\Phi_1) = \frac{1}{n}h_n(0)$.

2. The heralding rate is given by

$$h_n(\epsilon) = h_n(0) - (n-1)h_n(0)\epsilon + O(\epsilon^2). \quad (\text{III.7})$$

Proof. The first claim is proven in Appendix B3. The second claim follows from the first and

(III.4)-(III.6). □

Then up to first order in ϵ , the heralding rate is entirely governed by the ideal heralding rate $h_n(0)$. The ideal heralding rate in the Fourier and Hadamard cases is characterized as follows. In Appendix C, we compare these results to the case of Haar random linear optical unitaries.

Theorem III.4. *Let $U = F_n$ ($n \geq 3$) or $U = H_n$ ($n = 2^r \geq 4$). More generally, we may take U to be any $n \times n$ unitary with entries in the first row identically equal to $1/\sqrt{n}$.*

1. *The ideal heralding rate has the following equivalent expressions:*

$$h_n(0) = \left(\frac{-1}{n}\right)^{n-1} (n-1)! \sum_{t=0}^{n-1} (n-t) \frac{(-n)^t}{t!} \quad (\text{III.8})$$

$$= {}_2F_0(-(n-1), 2; 1/n), \quad (\text{III.9})$$

where ${}_2F_0(a, b; z) = \sum_{j \geq 0} \frac{(a)_j (b)_j}{j!} z^j$ is the generalized hypergeometric function, with $(a)_j = a(a+1) \cdots (a+j-1)$.

2. $\lim_{n \rightarrow \infty} h_n(0) = 1/4$.

The proof of the first equality in Part 1 is given in Appendix B 1 a; the second follows from reindexing $t \mapsto n-1-j$ and rewriting the terms. Part 2 follows from a result of Vaclav Kotesovec [25], proven using the Maple library *gdev* [26]. We adapt this proof to our setting in Appendix B 1 b.

Remark III.5. *We note that $\{n^{n-1}h_n(0)\}_{n \geq 1}$ is visibly a sequence of integers. Kotesovec entered the same sequence into The On-Line Encyclopedia of Integer Sequences as sequence A277458 in 2016 [25], as the coefficients of an exponential generating function related to the Lambert W function. The asymptotic above is given in the encyclopedia listing, up to the factor of n^{n-1} . We note that the W function appears in many physical problems [27], and certain variants were recently used in proposed protocols for verification of Gaussian boson sampling [28].*

The hypergeometric expression allows for quick numerical estimation of the ideal heralding rate. The first few values are $h_3(0) = 1/3$, $h_4(0) = 1/4$, $h_5(0) \approx 0.264$. In Figure 4, we plot the difference $h_n(0) - 1/4$ and numerically observe that $h_n(0)$ quickly approaches $1/4$, with asymptotic $h_n(0) - 1/4 \sim \frac{1}{16n}$. In particular, we conjecture

Conjecture III.6. *For $n \geq 5$, the sequence $h_n(0)$ monotonically decreases to $1/4$.*

As an immediate consequence of Theorems III.3 and III.4, we have:

Proposition III.7. *For $n \geq 4$ and sufficiently small ϵ ,*

$$h_n(\epsilon) \approx \frac{1}{4} - \left(\frac{n-1}{4}\right) \epsilon. \quad (\text{III.10})$$

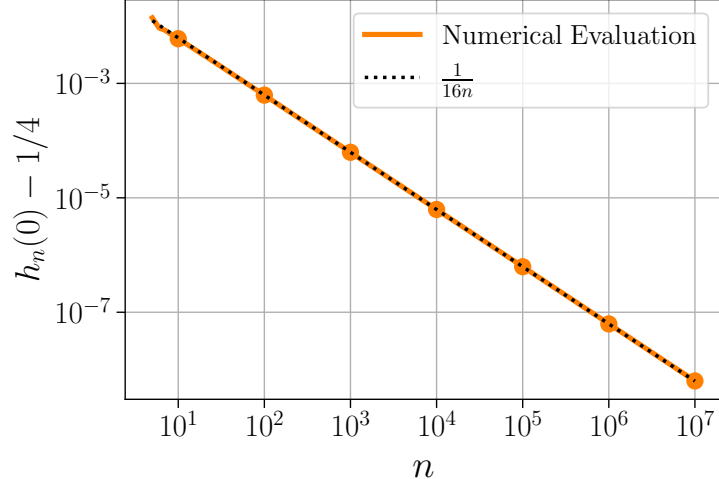


FIG. 4: Numerical evaluation of $h_n(0) - 1/4$ for $n = 5$ up to 10^7 . The data (solid line) contains all values of $n \in [5, 10^5]$, as well as multiples of 10^5 up to 10^6 , and multiples of 10^6 up to 10^7 (we include circular data points at powers of 10 to guide the eye). This was computed using the hypergeometric function, Eq. (III.9). We observed numerically that the deviation of $h_n(0)$ from $1/4$ falls as $1/(16n)$, plotted as the dashed line.

In Figure 5, we numerically plot heralding rates as a function of ϵ for the Fourier case. This plot, and others in this work, are obtained by numerically calculating the terms $h_n(\Phi_k)$, $0 \leq k \leq n$, and substituting into (III.4)-(III.6). Thus we obtain $h_n(\epsilon)$ as a polynomial in ϵ with explicitly known coefficients, up to rounding errors in the calculations for $h_n(\Phi_k)$. No sampling or fitting with respect to particular values of ϵ is required. In Appendix D, we explicitly give a list of computed heralding rates and output error rates as functions of ϵ . We see from Figure 5 that the protocol with $n = 3$ has a significantly better heralding rate than the larger protocols; however, as observed in Theorem III.2, the larger protocols have better output error rates for small ϵ . Further, since the heralding rate $h_n(0)$ stabilizes at $1/4$, it seems that for small ϵ it is advantageous to increase the value of n .

We use a similar expansion to the above, discussed in Appendix B, to calculate the output error rates $e_n(\epsilon)$, plotted in Fig. 2. We note that as ϵ grows larger, it is not necessarily better to increase n ; this is especially clear in Figs. 3 and 6. We further discuss the tradeoffs between different protocols in Section III C.

C. Comparison of resource costs

We now compare the resource costs of our distillation protocols with previous work. In particular, we consider the expected number of photons required to obtain output error rate $\epsilon' \approx \epsilon/n$ in the small ϵ regime.

The first photon distillation protocol, due to Sparrow and Birchall and called HOM filtering [4], requires n photons per distillation attempt, with heralding probability decaying exponentially to 0 [8]. Thus the expected number of photons required is exponential in n . If instead one iterates

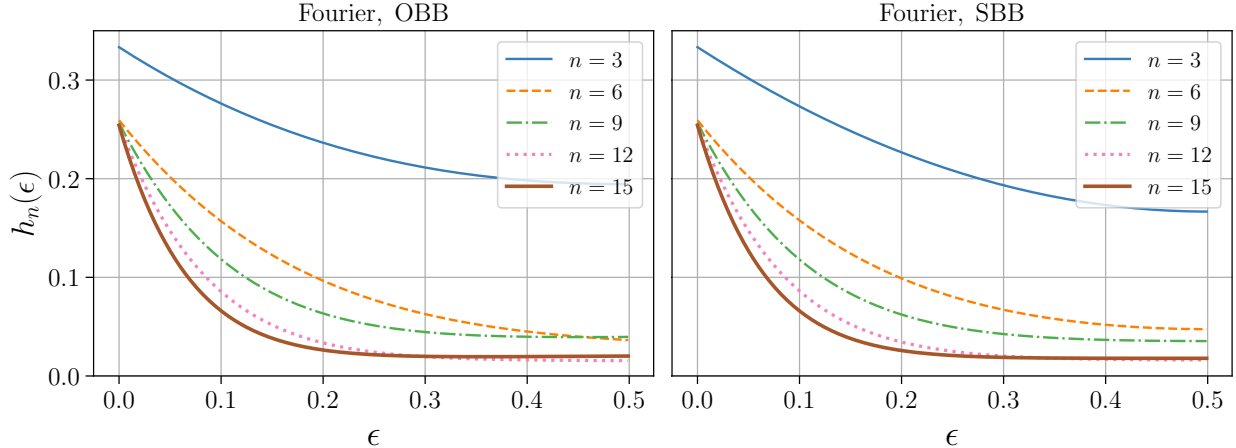


FIG. 5: Plot of the heralding rate $h_n(\epsilon)$ with OBB (left) and SBB (right) error models for the Fourier distillation protocol. The zero-error heralding rate $h_n(0)$ is given analytically by Th. III.4.

the 2-photon version of this scheme with active feed-forward, it is possible to have a scheme that scales cubically $O(n^3)$, as pointed out in [8].

Marshall [8] proposed the 3-photon Fourier distillation scheme and suggested iterating the scheme to arbitrarily reduce the error rate at the cost of additional photons. In particular, many batches of photons with error rate ϵ are put through a 3-photon distillation protocol, giving photons with output error rate near $\epsilon/3$ upon successful heralding; these then undergo further rounds of distillation to obtain error rate approximately $\epsilon/3^2$, then $\epsilon/3^3$, and so on. Without active feed-forward, it is easy to see that the expected number of photons to obtain output error rate $\epsilon' \approx \epsilon/n$ (where n is a power of 3) is exponential in n . With active feed-forward between rounds of distillation, this iterated distillation protocol can be made more efficient, with the number of photons scaling quadratically in n .

In our present setting, the n -photon protocol obtains output error rate $e_n(\epsilon) \approx \epsilon/n$ upon successful heralding in the small ϵ regime. The heralding rate satisfies $h_n(0) \approx 1/4$ for $n \geq 4$ (see Theorem III.4 and the following discussion). Then we have:

Theorem III.8. *For sufficiently small ϵ relative to n , the expected number of photons required to distill a single output photon with error rate $e_n(\epsilon) \approx \epsilon/n$ is*

$$\frac{n}{h_n(\epsilon)} \approx \frac{n}{h_n(0)} \approx 4n. \quad (\text{III.11})$$

In particular, our n -photon distillation protocol requires only *linearly scaling resources* to obtain the target error in the low ϵ regime. Thus the new protocols are the most resource-efficient known method for distilling the distinguishability error rate to an arbitrarily small value.

We recall, however, that our protocols for large n have an ever-decreasing *threshold* after which the protocol fails to reduce the distinguishability error rate. (See Figure 3.) In particular, in the discussion above, one must take ϵ sufficiently small so that it is below the threshold for all relevant values of n . This limitation does not apply to the iterated protocol of [8], as the relevant threshold is that of the 3-photon protocol. We note that these thresholds are not a major concern

for moderately sized protocols: as discussed above, we expect realistic experimental protocols to have $\epsilon \leq 0.15$ or so, below threshold for all $n \leq 16$, as seen in Figure 3.

However, even below the threshold, we may not always want to choose the largest value of n available. This is discussed in Section III E, especially Figures 6 and 7, where, for each ϵ , we numerically identify the value of n with smallest output error rate $e_n(\epsilon)$. If the initial error rate ϵ is large, we note that one may iterate Fourier (or Hadamard) distillation protocols with gradually increasing numbers of photons. The first rounds will have small n , chosen according to the figures, allowing for the reduction of the distinguishability error rate. Once the error rate is sufficiently small, one may use larger protocols in later rounds, further decreasing the error rate at a lower cost. For example, given initial $\epsilon_0 = 0.15$, applying the protocol with $U = F_6$ will give output error rate $\epsilon'_0 = e_6(\epsilon_0) \approx 0.056$ in the OBB model. (Calculated using the exact formula for $e_6(\epsilon)$ in Appendix D.) If a smaller error rate is required, we may then insert the output photons with error rate ϵ'_0 into the $U = F_{12}$ protocol, giving output error rate $\epsilon''_0 = e_{12}(\epsilon'_0) \approx 0.0097$.

D. Symmetries and conjectures

In this section, we briefly discuss the importance of certain symmetry properties to our results. We will return to this subject in much greater detail in Appendix A.

We consider a distillation protocol determined by $n \times n$ matrix U . We refer to a *mode symmetry* of U to be an $n \times n$ permutation matrix P such that there exists an $n \times n$ diagonal matrix D with $UP = DU$. In a boson sampling experiment, this corresponds to the observation that permuting the *modes* (not the photons) of the input state is equivalent to applying phase shifts on the output state. Let G be an abelian group of such mode symmetries for U . One can show that such symmetries lead to suppression laws [18]; in other words, we obtain a set \mathcal{S}_G of patterns (n_0, \dots, n_{n-1}) , determined by the symmetry group G , such that

$$\langle n_0, \dots, n_{n-1} | \hat{U} | 1, \dots, 1 \rangle \neq 0 \implies (n_0, \dots, n_{n-1}) \in \mathcal{S}_G. \quad (\text{III.12})$$

In a distillation setting, recalling (III.1), we see that the *ideal patterns* must be a subset of \mathcal{S}_G . As discussed above, in the Hadamard case, the ideal patterns may be exactly identified as the elements of \mathcal{S}_G (satisfying our additional restriction $n_0 = 1$) [17, 18]. In the Fourier case, we say that patterns in \mathcal{S}_G satisfy the *Zero Transmission Law* (ZTL), and the ideal patterns are in general a proper subset of the ZTL patterns [21]. The first non-ideal pattern satisfying the ZTL occurs for $n = 6$ (see Appendix A 2). In general, not all suppression laws may be explained by symmetry conditions such as the ZTL [29]: we expect that the extra suppression for $U = F_6$ is such a case. However, in Appendix A 2 a, we prove the following theorem:

Theorem III.9. *If n is a prime power, the suppression laws for $U = F_n$ are exactly characterized by the Zero Transmission Law. In particular, the ideal patterns (n_0, \dots, n_{n-1}) for $U = F_n$ are precisely the elements of \mathcal{S}_G with $n_0 = 1$.*

Beyond constraining the ideal patterns, these symmetries may be used to simplify calculations

for heralding and output error rates. In particular, we have the following, proven in Appendix A.

Theorem III.10. *Let U be an $n \times n$ unitary with corresponding symmetry group G and set \mathcal{S}_G of symmetry-preserving patterns. Let $|\eta\rangle \in \mathcal{H}^{\otimes n}$ be an arbitrary pure state, with normalized projection $|\eta_+\rangle$ onto the space of G -symmetric states. We have the following results.*

1. *Overlap with states in \mathcal{S}_G may be calculated in terms of the symmetrized state $|\eta_+\rangle$:*

$$\langle n_0, \dots, n_{n-1} | \hat{U} |\eta\rangle = \langle \eta_+ | \eta \rangle \langle n_0, \dots, n_{n-1} | \hat{U} |\eta_+\rangle.$$

2. *The heralding and error rates may be calculated in terms of the symmetrization:*

$$h_n(|\eta\rangle\langle\eta|) = |\langle \eta_+ | \eta \rangle|^2 h_n(|\eta_+\rangle\langle\eta_+|), \quad (\text{III.13})$$

$$e_n(|\eta\rangle\langle\eta|) = e_n(|\eta_+\rangle\langle\eta_+|). \quad (\text{III.14})$$

3. *Further assume that $U = H_n$, where n is a power of 2, or $U = F_n$, where n is a prime power. Then*

$$h_n(|\eta_+\rangle\langle\eta_+|) = |(\langle 1 | \otimes I) \hat{U} |\eta_+\rangle|^2. \quad (\text{III.15})$$

In particular, this gives a method for calculating heralding rates $h_n(|\eta\rangle\langle\eta|)$ while only checking whether output patterns have 1 photon in the output mode, rather than verifying whether the entire pattern is ideal. In Appendix B 2, we express $e_n(|\eta\rangle\langle\eta|)$ in a similar form involving only measurements on the 0th mode.

Remark III.11. *We briefly comment on the assumption on U in part 3 above. More generally, we can replace this with the assumption that all patterns (n_0, \dots, n_{n-1}) in \mathcal{S}_G with $n_0 = 1$ and $\langle n_0, \dots, n_{n-1} | \hat{U} |\eta\rangle \neq 0$ are ideal. As discussed above, this is automatically satisfied for U as in the theorem, as all patterns in \mathcal{S}_G with $n_0 = 1$ are ideal. For $|\eta\rangle = |1, \dots, 1\rangle$ perfectly indistinguishable, (III.15) follows from the definition of ideal pattern regardless of the unitary U , allowing for the straightforward computation of $h_n(0)$ as in Appendix B 1 a. Further, we show in Appendix B 3 that we may use the indistinguishable case to calculate $h_n(\Phi_1)$ in the cases $U = F_n, H_n$ regardless of n . In the Fourier case with n not a prime power, one may modify Protocol III.1 to post-select for any patterns in \mathcal{S}_G with $n_0 = 1$ rather than the smaller set of ideal patterns, so that the general assumption given above holds by definition. This intentionally increases the output error rate, but allows for the application of Theorem III.10 Part 3 and makes the behavior of the protocol more predictable for all n . Noting Figure 6, however, we advise against doing this, as the Fourier protocols with n not a prime power generally seem to be optimal without this modification.*

These symmetry considerations are essential in the proofs given in the Appendix. Further, they lead to the following conjectures:

Conjecture III.12. *As above, assume that $U = H_n$, where n is a power of 2, or $U = F_n$, where n is a prime power. Let $|\eta\rangle, |\Delta\rangle$ be states of the form (II.14), where $|\eta\rangle$ has k distinguishability*

errors and $|\Delta\rangle$ has n (so that in the latter case, all photons are mutually fully distinguishable). Let $|\eta_+\rangle, |\Delta_+\rangle$ be the G -symmetrizations, as above. Then

$$h_n(\Phi_0) \leq h_n(|\eta_+\rangle\langle\eta_+|) \leq h_n(|\Delta_+\rangle\langle\Delta_+|). \quad (\text{III.16})$$

In particular,

$$\frac{1}{n}h_n(\Phi_0) \leq h_n(\Phi_k) \leq \frac{\gcd(k, n)}{n}h_n(|\Delta_+\rangle\langle\Delta_+|). \quad (\text{III.17})$$

The heart of this conjecture is that for G -symmetrized states, more mode symmetry seems to *decrease* the heralding rate. Thus the lower bound comes from the fully mode-symmetric state $\Phi_0 = |1, \dots, 1\rangle\langle 1, \dots, 1|$ and the upper bound from a state $|\Delta\rangle$ with as little symmetry as possible. The coefficients come from Theorem III.10 Part 2 and trivial bounds on $|\langle\eta_+|\eta\rangle|^2$ when $|\eta\rangle$ has k distinguishability errors.

For F_n where n is not a prime power, the conjecture fails, with such protocols tending to have lower heralding rate than predicted: for example, in the OBB model we have $h_6(\Phi_2)/h_6(\Phi_0) \approx 0.132 < 1/6$. However, the conjecture seems to hold for general F_n if we modify the protocol as suggested in Remark III.11. With this modification, we would for example have $h_6(\Phi_2)/h_6(\Phi_0) \approx 0.216 > 1/6$, and the $n = 6$ case would then fit into the same patterns as the prime-power cases. (But this would negatively impact the error rate, e.g., increasing $e_6(\Phi_2)$ from 0.017 to 0.026).

As a corollary of the previous conjecture, we obtain the following:

Conjecture III.13. *For the n -photon Fourier or Hadamard protocols, with n a prime power as above, we have*

$$h_n(\epsilon) \geq h_n(0) \left((1 - \epsilon)^n \left(1 - \frac{1}{n} \right) + \frac{1}{n} \right). \quad (\text{III.18})$$

In particular, if $\epsilon \leq \frac{1}{n}$, by Theorem III.4 we have

$$\lim_{n \rightarrow \infty} h_n(\epsilon) \geq \lim_{n \rightarrow \infty} h_n(0) \left(\left(1 + \frac{1}{n} \right)^{n+1} + \frac{1}{n} \right) = \frac{1}{4e} \approx 0.092. \quad (\text{III.19})$$

Then assuming the conjecture holds, we see that as long as ϵ is small relative to n , the heralding rates cannot get too small even for large n . Further, if Conjecture III.6 holds, we have for all $n \geq 3$

$$h_n(\epsilon) \geq \frac{1}{4e}. \quad (\text{III.20})$$

Recall from our earlier discussion of error thresholds that choosing n and ϵ appropriately is also important to ensure that the distillation protocols reduce error rates. Here we note that the numerical threshold values obtained in Figure 3 are all far greater than $1/n$. Thus it appears that if $\epsilon < 1/n$, we obtain both a large heralding rate and a distillation protocol that improves the output error rate.

E. Numerics

In this section, we give further numerics for our protocols.

First, we consider the question of optimal distillation protocols given an error rate ϵ . In particular, as discussed in Section III C, we expect the heralding rates of our protocols to be reasonably large, with linearly growing resource requirements. The limitation is instead the growth of the error rate: protocols with large n give the smallest output error rate when ϵ is small, but perform worse for large ϵ . Thus, in Figure 6, we consider all protocols with $U = F_n$, $3 \leq n \leq 16$, and for each ϵ determine the value of n with $e_n(\epsilon)$ as small as possible. We are most interested in $\epsilon \leq 0.15$, as discussed above. As expected, we find that the largest protocol is optimal for small ϵ , and as ϵ grows the optimal protocol becomes smaller and smaller. Further, in the OBB model, there is a large plateau for ϵ roughly between 0.1 and 0.4 in which the 6-photon protocol is optimal. We expect this is due to the fact for $n = 6$, the set of ideal patterns is strictly smaller than the set of symmetry-preserving patterns, as discussed in Section III D and Appendix A 2. In fact, for both error models and reasonably small values of ϵ , the dominant protocols seem to have $n = 6, 12, 15$, all of which are not prime powers and have a set of ideal patterns strictly smaller than the set of symmetry-preserving patterns [16] (recall Theorem III.9). (Note we exclude $n = 16$ from the discussion here, as by Theorem III.2 it is guaranteed to be optimal for sufficiently small ϵ .) The strong performance of $n = 6, 12, 15$ is unsurprising, since a smaller set of ideal patterns leads to a smaller heralding rate: see the discussion below Conjecture III.12. As explained in more detail below, this should generally reduce the error rate as well. We also note that these seemingly optimal protocols have n divisible by 3. Understanding this divisibility condition may explain why there is no point at which $n = 14$ is preferable to $n = 12$ or $n = 15$, even though all three have fewer ideal patterns than symmetry-preserving patterns. In Figure 7, we repeat this analysis while including the Hadamard protocols as well. We find that for reasonably small values of ϵ , the same Fourier protocols (n not a prime power and divisible by 3) are generally preferred. (The fact that H_{16} is preferred over F_{16} in the OBB model seems to be related to the discussion of the $n = 8$ case below.) We conjecture that if we included all $n \leq 18$ in the analysis, we would see the optimal protocol transition directly from F_{18} to F_{15} or F_{12} .

In the preceding analysis, we compared protocols with different values of n . Next, we fix $n = 8$ and numerically investigate the heralding and error rates of the distillation protocols using different unitaries and error models. We choose to study $n = 8$ here because it is a power of 2, allowing for comparison of corresponding Fourier and Hadamard distillation protocols. The $n = 4$ case was originally presented in [8], so $n = 8$ is the smallest new case relevant to both protocols. We note that similar results to the below hold for the $n = 4$ case. For this discussion, we note the following formula for the output error rate, given in Appendix B 2:

$$e_n(\epsilon) = \frac{\bar{e}_n(\epsilon)}{h_n(\epsilon)} = \frac{\sum_{k=1}^n \binom{n}{k} \epsilon^k (1-\epsilon)^{n-k} e_n(\Phi_k) h_n(\Phi_k)}{\sum_{k=0}^n \binom{n}{k} \epsilon^k (1-\epsilon)^{n-k} h_n(\Phi_k)}. \quad (\text{III.21})$$

We recall that $e_n(\Phi_k)$ is a conditional probability: the probability that, if a state with k distinguishability errors leads to an ideal pattern, it outputs a non-ideal photon. Recalling Theorems

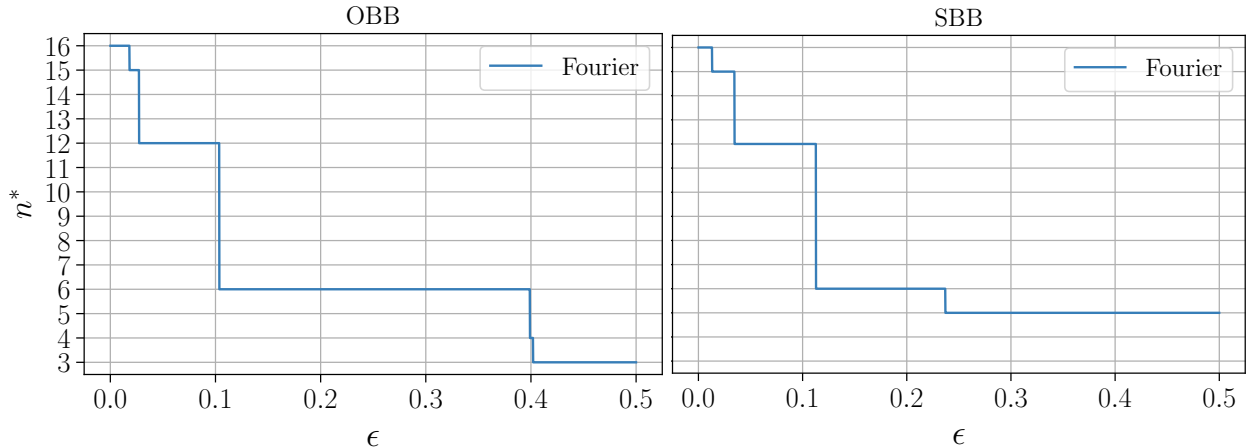


FIG. 6: Given an initial error rate ϵ , we plot the value n^* of n for which the the protocol with $U = F_n$ gives the greatest error reduction (this does not take into account heralding rates or expected resource counts). We considered protocols up to size $n = 16$. As expected, for small ϵ we have $n^* = 16$, since $e_n(\epsilon) \approx \epsilon/n$.

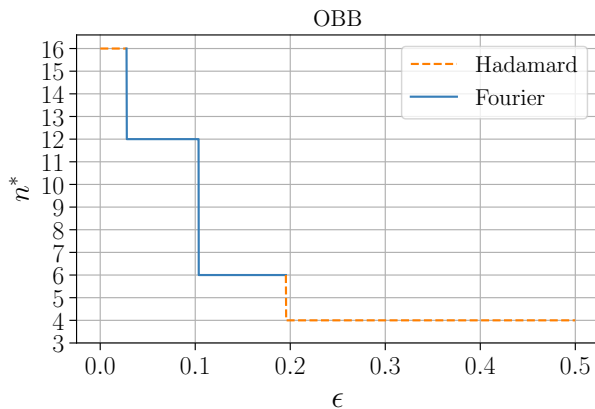


FIG. 7: We extend the plot of Figure 6 (OBB) to include the Hadamard protocols $U = H_4, H_8, H_{16}$. The different line styles indicate whether the protocol of interest is Fourier or Hadamard. Note that in the SBB case, the plot is unchanged from the one in Figure 6 (i.e., for the SBB error model, the Fourier protocol always has the greatest error reduction).

III.2, III.3, and III.4, the quantities $h_8(\Phi_0), h_8(\Phi_1), e_8(\Phi_1)$ are fixed and we have the first-order approximations

$$e_8(\epsilon) = e_8(\Phi_1)\epsilon + O(\epsilon^2), \quad h_8(\epsilon) = h_8(\Phi_0)(1 - 7\epsilon) + O(\epsilon^2), \quad (\text{III.22})$$

regardless of the error model or the choice of $U \in \{F_8, H_8\}$. Then we expect much of the difference between protocols and models to be explainable via the second-order terms, which are determined by $h_8(\Phi_2), e_8(\Phi_2)$ in addition to the above fixed quantities. In particular, $e_8(\Phi_2)$ and $h_8(\Phi_2)$ affect the numerator of (III.21) to second order; $h_8(\Phi_2)$ also affects the denominator, but only to third order. We give values for these second-order quantities in Table I. One may think of Φ_2 in the OBB

model as an average of all states with 2 “different” errors; in the SBB model, Φ_2 is an average of states with 2 of the “same” error.

	$h_8(\Phi_2)$	$e_8(\Phi_2)$
Fourier, OBB	0.040	0.377
Fourier, SBB	0.042	0.328
Hadamard, OBB	0.038	0.338
Hadamard, SBB	0.076	0.338

TABLE I: We plot the values of $h_8(\Phi_2)$ and $e_8(\Phi_2)$ for the variant protocols and error models considered here. These are the dominant values that differ between cases, and they determine the behavior of $h_8(\epsilon)$, $e_8(\epsilon)$ up to second order.

In Figure 8, we plot the heralding rates and output error rates in the Fourier and Hadamard cases, using both the OBB and SBB error models. We are particularly interested in the small ϵ regime. We note from the plot that 3 of the 4 cases considered have very similar heralding rates $h_8(\epsilon)$. The Hadamard case with SBB error model, however, has a significantly larger heralding rate. This is clearly reflected in the values of $h_8(\Phi_2)$ in Table I, with the Hadamard SBB case nearly doubling the other values. Since the only second-order effect of $h_8(\Phi_2)$ on (III.21) is in the numerator, an increase in this quantity should increase the overall error rate. This explains why this case has significantly worse error rate than the others, as seen in Figure 8. Intuitively, the Hadamard protocol does not notice two of the “same” (SBB) errors as often, so we are more likely to have distinguishable output photons.

Remark III.14. *We reiterate the above observation: even though a large heralding rate reduces the overall resource requirements, it can also lead to larger error rates. This is what makes our protocols notable, especially as n increases: they maintain a nontrivial heralding rate while arbitrarily decreasing the error rate.*

Next, we fix an error model and compare error rates $e_n(\epsilon)$ for F_n and H_n . For SBB, the Fourier case $U = F_8$ has smaller output error rate, translating to better performance. This is explained by the analysis above. When we consider the OBB error model, however, we see that the Hadamard protocol $U = H_8$ has the smaller error rate and better performance, with both $h_8(\Phi_2)$ and $e_8(\Phi_2)$ decreasing in this case. Then for a fixed $n = 2^r$, we cannot conclude whether Fourier or Hadamard unitaries are preferable in general: this depends strongly on the error model relevant to the experiment in question. Note that this is in contrast with the discussion of Figures 6 and 7 above, in which we found that Fourier protocols often perform better when we are free to choose the value of n .

Similarly, we may fix the unitary (Fourier or Hadamard) and compare the error rates $e_n(\epsilon)$ under the two error models. From Figure 8, we see that the Hadamard protocol performs better with OBB errors, whereas the Fourier protocol performs better with SBB errors. In the Hadamard case, this may be explained by the increased heralding rate under the SBB model, as discussed above. For $U = F_8$, however, the heralding rate does not significantly differ between the two error

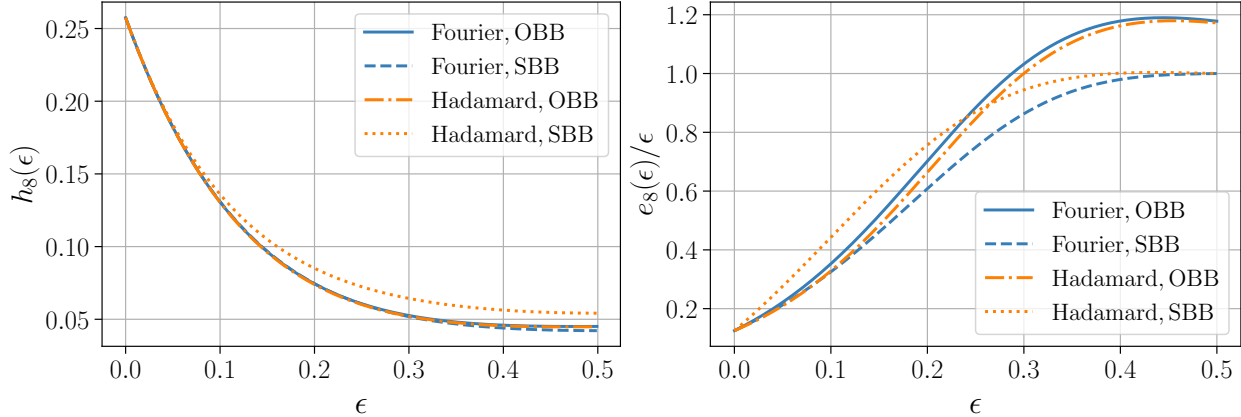


FIG. 8: Heralding rate (left) and output error rate (right) for $n = 8$ Fourier and Hadamard protocols, for both OBB and SBB noise models.

models. (In fact, the protocol with smaller error rate $e_n(\epsilon)$ has slightly *larger* heralding rate!) Then the discrepancy is caused by the change in $e_8(\Phi_2)$, which is proportionally more significant. Intuitively, for the F_8 protocol, states with 2 errors give ideal output patterns at roughly the same rate regardless of error model, but when heralding occurs and the errors are “different,” the error photons are more likely to end up in the output mode.

In summary, we note that Fourier protocols, especially those with n divisible by 3 and not a prime power, seem to be the most effective at reducing the error rate. For a fixed $n = 2^r$, however, whether F_n or H_n performs better seems to be highly dependent on the error model. Finally, the Hadamard protocols seem to struggle with filtering out SBB errors, while the Fourier protocols are equally capable of filtering out both types but, when heralding occurs, are more likely to direct OBB errors to the output mode.

F. Incorporation of photon loss

We now discuss the incorporation of photon loss models into our analysis of the Fourier and Hadamard distillation protocols. We begin with a brief discussion of loss models.

We initially consider the *uniform beamsplitter loss model*, in which our linear optical circuit is made up of lossy beamsplitters, and each photon has probability λ of loss at each beamsplitter. We model this as a photon loss channel with loss probability λ , occurring independently on each of the two relevant modes, just before the beamsplitter. We recall, however, that symmetric loss commutes through linear optics [30]. For the unitary $U = H_n$, we give an explicit recursive circuit decomposition in Figure 9, and note that the described loss channels may be commuted to the end of the circuit. In particular, since each path from an input mode to an output mode involves exactly $\log_2 n$ beamsplitters, the loss probability on each mode is $\Lambda = 1 - (1 - \lambda)^{\log_2 n}$. For simplicity, we consider the same loss model in the Fourier case. This may likely be derived as above; for example, when n is a power of 2, a circuit decomposition similar to that in Figure 9 is given in [31], and the same analysis holds. Then, going forward, we will use the *simplified loss model* depicted in

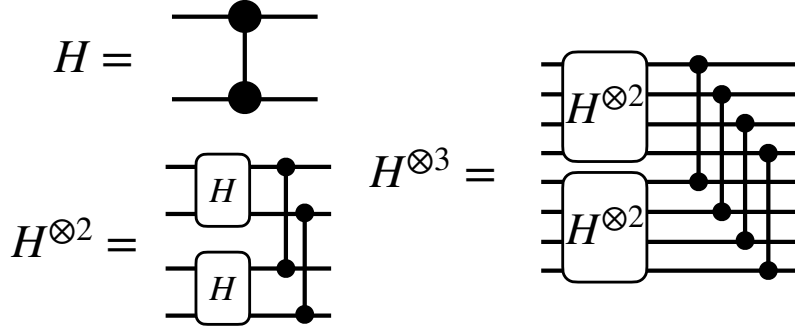


FIG. 9: Illustration of construction of the circuit implementing the $n \times n$ Hadamard unitaries $H_n = H^{\otimes r}$, for $r = 1, 2, 3$, where $n = 2^r$. It generalizes in the obvious way. The circuit components are 50:50 beamsplitters. One can see directly that each mode interacts with r beamsplitters.

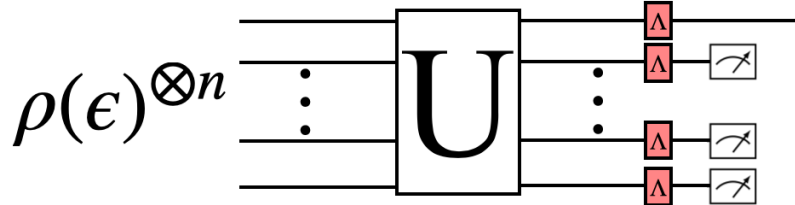


FIG. 10: Illustration of our error model. As in the rest of the paper, n partially distinguishable photons, each with internal state $\rho(\epsilon)$, are input into n different external modes, and we apply the linear optical unitary \hat{U} corresponding to an $n \times n$ unitary U . Unique to this section, we then apply a photon loss channel, with loss probability $\Lambda = 1 - (1 - \lambda)^{\log n}$, to each mode. We then perform PNRD on the final $n - 1$ modes and post-select as usual. For the Hadamard circuits of Figure 9, this is equivalent to the uniform beamsplitter loss model with probability λ of loss at each beamsplitter.

Figure 10, in which partially distinguishable photons are given as input to the circuit, the linear optical unitary \hat{U} is applied, each photon independently undergoes a loss channel with probability $\Lambda = 1 - (1 - \lambda)^{\log n}$, and the final $n - 1$ modes are measured. We note that in this model, the probability that no photons are lost is $(1 - \Lambda)^n = (1 - \lambda)^{n \log n}$.

We begin by discussing the heralding rate, which we now write as $h_n(\epsilon; \lambda)$ to allow for dependence on the loss rate, with $h_n(\epsilon) = h_n(\epsilon; 0)$. Heralding requires the detection of $n - 1$ photons in the latter $n - 1$ modes; in particular, heralding is only possible if at most 1 photon has been lost. We have the corresponding decomposition

$$h_n(\epsilon; \lambda) = (1 - \Lambda)^n h_n(\epsilon) + \Lambda(1 - \Lambda)^{n-1} h_n^{(1)}(\epsilon), \quad (\text{III.23})$$

where $h_n(\epsilon) = h_n(\epsilon; 0)$ encapsulates the heralding probability when no photons are lost and $h_n^{(1)}(\epsilon)$ is the heralding probability when exactly 1 photon is lost (as mentioned above, $h_n^{(k)}(\epsilon) = 0$ for $k > 1$). Note that we have two possibilities for pre-loss output patterns contributing to $h_n^{(1)}(\epsilon)$: either we have an ideal pattern and the single photon in mode 0 is lost; or we have a *non-ideal* pattern, and a photon in a nonzero mode is lost, and the resulting pattern on the final $n - 1$ modes

matches an ideal pattern. In either case, no photons exit mode 0. From this description, we see that $h_n^{(1)}(\epsilon) \geq h_n(\epsilon)$, because $h_n(\epsilon)$ counts only the terms contributing to the first case described above. This gives a lower bound on the heralding rate:

Theorem III.15. *Let all notation be as above. For the Fourier or Hadamard protocols, we have*

$$h_n(\epsilon; \lambda) \geq (1 - \Lambda)^{n-1} h_n(\epsilon) = (1 - \lambda)^{(n-1) \log n} h_n(\epsilon). \quad (\text{III.24})$$

If $\epsilon = 0$, the bound is tight:

$$h_n(0; \lambda) = \Lambda^{n-1} h_n(0) = (1 - \lambda)^{(n-1) \log n} h_n(0). \quad (\text{III.25})$$

Proof. The first claim follows by bounding $h_n^{(1)}(\epsilon) \geq h_n(\epsilon)$ as above and substituting into (III.24). For the second claim, we argue that $h_n(0) = h_n^{(1)}(0)$. We recall that when $\epsilon = 0$, the (pre-loss) output patterns satisfy certain symmetry constraints, given in Section III A. In particular, in the notation used above, we have $\sum_i g_i \equiv 0 \pmod n$ in the Fourier case and $\bigoplus_i g_i = 0$ in the Hadamard case. For a non-ideal pattern to contribute to $h_n^{(1)}$, there must exist two symmetry-preserving patterns of n photons in n modes, one ideal and one non-ideal, both of which may give the same $(n - 1)$ -photon pattern after a loss. The symmetry conditions given above make this impossible: given a pattern of $n - 1$ photons in n modes, there is a unique mode j such that adding a photon to mode j results in a symmetry-preserving pattern. \square

This may be used to obtain an upper bound on the resources required for distillation in the presence of loss. With a nonzero loss rate λ , the heralding rate is exponentially suppressed in $n \log n$, leading to exponentially growing resource requirements. Given a fixed amount of resources and error rates ϵ, λ , this effectively puts an upper bound on the maximum feasible size n of a distillation protocol. We show numerical scaling of the heralding probability in Fig. 11 for $n = 8$.

We now briefly discuss the output error rate. In the presence of photon loss, the definition of output error rate given in Section III A is no longer well-defined, as it assumes there is always 1 output photon. In the more general setting, it is more natural to consider the *output success rate* $f_n(\epsilon; \lambda)$ to be the probability that, given the heralding of an ideal pattern, there is a single output photon with internal state $|\xi_0\rangle$. (In other words, we count the probability of outputs with no photon loss *and* an ideal output photon.) The output error rate is then $e_n(\epsilon; \lambda) = 1 - f_n(\epsilon; \lambda)$. We note that $f_n(\epsilon; \lambda)$ is straightforwardly computable in terms of the quantities we have already discussed. In particular, since successful output requires no photon loss,

$$f_n(\epsilon; \lambda) = P(\text{no loss} | \text{herald}) f_n(\epsilon; 0) \quad (\text{III.26})$$

$$= \frac{(1 - \lambda)^{n \log n} h_n(\epsilon; 0)}{h_n(\epsilon; \lambda)} f_n(\epsilon; 0), \quad (\text{III.27})$$

where the second equality follows from Bayes' theorem.

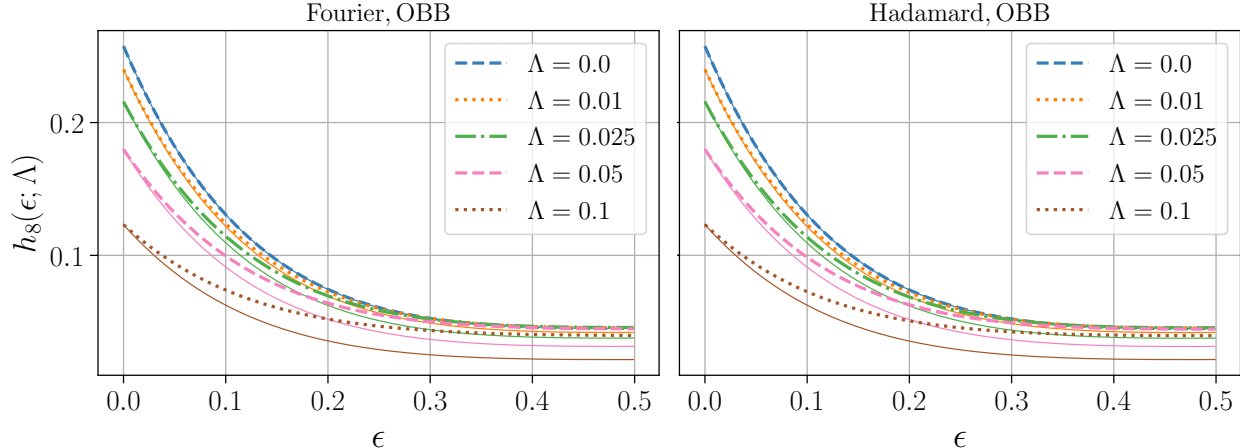


FIG. 11: Heralding probability with photon loss in the Fourier (left) and Hadamard (right) protocols, for $n = 8$, with the OBB error model. The SBB curves look similar. Note that the parameter in the legend is $\Lambda = 1 - (1 - \lambda)^{\log n}$. The thin solid lines represent the lower bound, Eq. (III.24), and notice they intersect the data curves at $\epsilon = 0$ as per Eq. (III.25). We see the lower bound is tighter for smaller Λ .

IV. DISCUSSION

We have provided a set of protocols for reducing photonic distinguishability errors, using n photons to reduce the error rate by a factor of n . This generalizes the work of [4, 8]. Our protocols, based on the Hadamard and Fourier unitaries, can scale to arbitrarily many photons (in contrast to [8]) and retain a high heralding probability near $1/4$ even for large n (in contrast to [4]). These protocols are efficient in the sense that they require $O(n)$ photons to reduce the error by a factor of n , an improvement over [4, 8].

We proved and conjectured several results about these protocols, including giving lower bounds on the heralding rates in Sections III B and III D, characterizing the effect of photon loss in Section III F, and discussing resource costs and optimal choices of distillation protocols in Sections III C and III E. Much of this analysis was enabled by symmetries present in the Fourier and Hadamard matrices [18], which is also related to the efficiency of these protocols.

We also show in App. C that while distillation is *possible* using almost any unitary (in particular for Haar random unitaries), it does not yield an efficiently scaling protocol. First we observe that in the Haar case (as with Fourier/Hadamard), the heralding rate for the ideal patterns asymptotically approaches $1/4$ (the ‘ideal’ patterns in the Haar case are typically just all possible patterns as there’s no symmetry). However, in the Haar case, post-selecting on all ideal patterns increases the error (approximately doubling it). Instead, Haar random unitaries can be used for distillation only when one chooses the post-selection patterns as a small subset of ideal patterns with a high amount of constructive interference (high probability). Although the Haar case does not scale efficiently, these observations help to highlight how the Hadamard/Fourier protocols achieve efficiency; the symmetry causes a concentration on a relatively small number of possible patterns, as demonstrated in Fig. 12. This figure shows that in the Fourier case, the total proportion of ideal patterns (out of all possible ones) scales like $1/n$, as expected from analysis in Ref. [21]. Remarkably, the weight

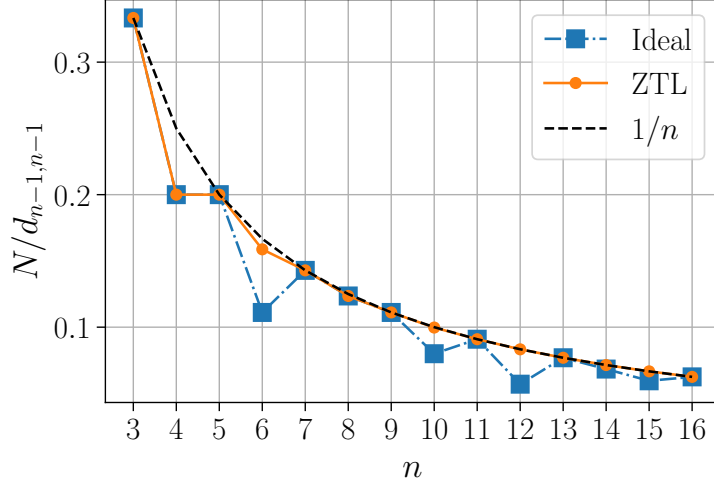


FIG. 12: For the Fourier matrices F_n , we plot the ratio of the total number N of ideal patterns (respectively, ZTL patterns with 1 photon in mode 0) to the total number of possible patterns $d_{n-1, n-1}$ (dimension of the space of $n-1$ photons in $n-1$ modes). As expected from [21], it scales like $1/n$. We can also see here that for prime powers, the ZTL patterns match the ideal ones (see Th. III.9), but for non-prime powers there are likely additional suppression laws.

of these patterns remains approximately constant, at $1/4$, as proven in Theorem III.4.

We proved in Theorem III.9 that for n a prime power, the Fourier protocols (like the Hadamard protocols [17]) have ideal patterns exactly characterized by symmetry. However, not all suppression laws come from symmetry conditions [29]. In particular, our numerical analysis in Section III E indicates that the optimal distillation protocols correspond to F_n where n is *not* a prime power. (See Figure 6.) In all such cases we considered, the ideal patterns are a strict subset of those determined by the known symmetry conditions. Further, there seem to be additional properties determining which $n \neq p^r$ lead to optimal distillation protocols: for example, F_n with n divisible by 3 seem to outperform other non-prime-power n . Thus we believe that future work on distillation should focus on understanding and taking advantage of the extra suppression occurring in these cases.

V. ACKNOWLEDGEMENTS

We are grateful for support from the NASA SCaN program, from DARPA under IAA 8839, Annex 130, and from NASA Ames Research Center. J.M. is thankful for support from NASA Academic Mission Services, Contract No. NNA16BD14C. N.A. is a KBR employee working under the Prime Contract No. 80ARC020D0010 with the NASA Ames Research Center. We also thank Vaclav Kotesovec for pointing out the proof of Theorem III.4 Part 2 discussed in Appendix B 1 b. The United States Government retains, and by accepting the article for publication, the publisher acknowledges that the United States Government retains, a nonexclusive, paid-up, irrevocable, worldwide license to publish or reproduce the published form of this work, or allow others to do

so, for United States Government purposes.

-
- [1] E. Knill, G. Ortiz, and R.D. Somma. “Optimal quantum measurements of expectation values of observables”. *Physical Review A* **75** (2007).
 - [2] D.E. Browne and T. Rudolph. “Resource-Efficient Linear Optical Quantum Computation”. *Physical Review Letters* **95**, 010501 (2005).
 - [3] S. Bartolucci, P. Birchall, H. Bombín, H. Cable, C. Dawson, M. Gimeno-Segovia, E. Johnston, K. Kieling, N. Nickerson, M. Pant, F. Pastawski, T. Rudolph, and C. Sparrow. “Fusion-based quantum computation”. *Nature Communications* **14**, 912 (2023).
 - [4] C. Sparrow. “Quantum Interference in Universal Linear Optical Devices for Quantum Computation and Simulation”. *Imperial College London* (2017).
 - [5] R.D. Shaw, A.E. Jones, P. Yard, and A. Laing. “Errors in heralded circuits for linear optical entanglement generation” (2023). url: <https://arxiv.org/abs/2305.08452>.
 - [6] J.J. Renema, A. Menssen, W.R. Clements, G. Triginer, W.S. Kolthammer, and I.A. Walmsley. “Efficient Classical Algorithm for Boson Sampling with Partially Distinguishable Photons”. *Physical Review Letters* **120**, 220502 (2018).
 - [7] P.J. Mosley, J.S. Lundeen, B.J. Smith, P. Wasylczyk, A.B. U’Ren, C. Silberhorn, and I.A. Walmsley. “Heralded Generation of Ultrafast Single Photons in Pure Quantum States”. *Physical Review Letters* **100**, 133601 (2008).
 - [8] J. Marshall. “Distillation of Indistinguishable Photons”. *Physical Review Letters* **129**, 213601 (2022).
 - [9] C.F.D. Faurby, L. Carosini, H. Cao, P.I. Sund, L.M. Hansen, F. Giorgino, A.B. Villadsen, S.N. van den Hoven, P. Lodahl, S. Paesani, J.C. Loredo, and P. Walther. “Purifying photon indistinguishability through quantum interference” (2024). [arXiv:2403.12866](https://arxiv.org/abs/2403.12866).
 - [10] M. Halder, A. Beveratos, R.T. Thew, C. Jorel, H. Zbinden, and N. Gisin. “High coherence photon pair source for quantum communication”. *New Journal of Physics* **10**, 023027 (2008).
 - [11] Y. Tsujimoto, Y. Sugiura, M. Tanaka, R. Ikuta, S. Miki, T. Yamashita, H. Terai, M. Fujiwara, T. Yamamoto, M. Koashi, M. Sasaki, and N. Imoto. “High visibility Hong-Ou-Mandel interference via a time-resolved coincidence measurement”. *Optics Express* **25**, 12069–12080 (2017).
 - [12] J.L. Tambasco, G. Corrielli, R.J. Chapman, A. Crespi, O. Zilberberg, R. Osellame, and A. Peruzzo. “Quantum interference of topological states of light”. *Science Advances* **4**, eaat3187 (2018).
 - [13] S. Wang, C.X. Liu, J. Li, and Q. Wang. “Research on the Hong-Ou-Mandel interference with two independent sources”. *Scientific Reports* **9**, 3854 (2019).
 - [14] H. Ollivier, S.E. Thomas, S.C. Wein, I.M. de Buy Wenniger, N. Coste, J.C. Loredo, N. Somaschi, A. Harouri, A. Lemaitre, I. Sagnes, L. Lanco, C. Simon, C. Anton, O. Krebs, and P. Senellart. “Hong-Ou-Mandel Interference with Imperfect Single Photon Sources”. *Physical Review Letters* **126**, 063602 (2021).
 - [15] F.H.B. Somhorst, R. van der Meer, M. Correa Anguita, R. Schadow, H.J. Snijders, M. de Goede, B. Kassenberg, P. Venderbosch, C. Taballione, J.P. Epping, H.H. van den Vlekert, J. Timmerhuis, J.F.F. Bulmer, J. Lugani, I.A. Walmsley, P.W.H. Pinkse, J. Eisert, N. Walk, and J.J. Renema. “Quantum simulation of thermodynamics in an integrated quantum photonic processor”. *Nature Communications* **14**, 3895 (2023).
 - [16] M.C. Tichy. “Sampling of partially distinguishable bosons and the relation to the multidimensional permanent”. *Physical Review A* **91**, 022316 (2015).

- [17] A. Crespi. “Suppression laws for multiparticle interference in Sylvester interferometers”. *Physical Review A* **91**, 013811 (2015).
- [18] C. Dittel, G. Dufour, M. Walschaers, G. Weihs, A. Buchleitner, and R. Keil. “Totally destructive interference for permutation-symmetric many-particle states”. *Physical Review A* **97**, 062116 (2018).
- [19] M.C. Tichy, K. Mayer, A. Buchleitner, and K. Mølmer. “Stringent and efficient assessment of boson-sampling devices”. *Physical review letters* **113**, 020502 (2014).
- [20] N. Viggianiello, F. Flamini, L. Innocenti, D. Cozzolino, M. Bentivegna, N. Spagnolo, A. Crespi, D.J. Brod, E.F. Galvão, R. Osellame, et al. “Experimental generalized quantum suppression law in Sylvester interferometers”. *New Journal of Physics* **20**, 033017 (2018).
- [21] M.C. Tichy, M. Tiersch, F. de Melo, F. Mintert, and A. Buchleitner. “Zero-transmission law for multiport beam splitters”. *Physical review letters* **104**, 220405 (2010).
- [22] M. Englbrecht, T. Kraft, C. Dittel, A. Buchleitner, G. Giedke, and B. Kraus. “Indistinguishability of identical bosons from a quantum information theory perspective”. *Physical Review Letters* **132**, 050201 (2024).
- [23] C. Sparrow. “Quantum interference in universal linear optical devices for quantum computation and simulation”. *PhD thesis* (2017).
- [24] J. Saied, J. Marshall, N. Anand, S. Grabbe, and E.G. Rieffel. “Advancing quantum networking: some tools and protocols for ideal and noisy photonic systems”. In *Quantum Computing, Communication, and Simulation IV*. Volume 12911, pages 37–65. SPIE (2024).
- [25] OEIS Foundation Inc. “Entry a277458 in the On-Line Encyclopedia of Integer Sequences” (2024). Published electronically at <https://oeis.org/A277458>.
- [26] B. Salvy. “Examples of automatic asymptotic expansions”. *ACM Sigsam Bulletin* **25**, 4–17 (1991).
- [27] S.R. Valluri, D.J. Jeffrey, and R.M. Corless. “Some applications of the Lambert W function to physics”. *Canadian Journal of Physics* **78**, 823–831 (2000).
- [28] F.V. Mendes, C. Lima, and R.V. Ramos. “Applications of the Lambert–Tsallis W_q function in quantum photonic Gaussian boson sampling”. *Quantum Information Processing* **21**, 215 (2022).
- [29] M.E.O. Bezerra and V. Shchesnovich. “Families of bosonic suppression laws beyond the permutation symmetry principle”. *New Journal of Physics* **25**, 093047 (2023).
- [30] M. Oszmaniec and D.J. Brod. “Classical simulation of photonic linear optics with lost particles”. *New Journal of Physics* **20**, 092002 (2018).
- [31] R. Barak and Y. Ben-Aryeh. “Quantum fast Fourier transform and quantum computation by linear optics”. *JOSA B* **24**, 231–240 (2007).
- [32] S. Aaronson and A. Arkhipov. “The computational complexity of linear optics”. In *Proceedings of the forty-third annual ACM symposium on Theory of computing*. Pages 333–342. (2011).
- [33] S. Akbari, H.R. Fanai, and K. Mahmoudian. “On the matrices with constant determinant and permanent over roots of unity”. *Linear algebra and its applications* **375**, 245–249 (2003).
- [34] M. Ledoux. “The Concentration of Measure Phenomenon”. <https://www.ams.org/surv/089> (2005).

Appendix A: Symmetry

1. General case

In this section, we review an argument due to [18] to show that certain types of symmetries of a unitary U determine the transition probabilities of the associated linear optical unitary \hat{U} . Suppose we have an $n \times n$ unitary U . As above, we write $\hat{U}|\psi\rangle$ to denote the action of the corresponding linear optical unitary on the state $|\psi\rangle \in \mathcal{H}^{\otimes n}$. In this section, we only consider PNRD. As shorthand, we write $\langle s_0, \dots, s_{n-1}|$ for the projector onto the subspace of states with s_j photons in mode j . (Regardless of internal states.) Thus we will be interested in the transition probabilities $\langle s_0, \dots, s_{n-1}|\hat{U}|\psi\rangle$.

Suppose there is some $n \times n$ permutation matrix P such that $UP = DU$, where D is a diagonal matrix with diagonal entries d_0, \dots, d_{n-1} . (By unitarity, all $|d_i| = 1$.)

Remark A.1. *Before continuing, we emphasize that the linear optical unitary \hat{P} is a permutation of the external modes of the input state, acting by $P^{\otimes n} \otimes I^{\otimes n}$ on $\mathcal{H}_{\text{ext}}^{\otimes n} \otimes \mathcal{H}_{\text{int}}^{\otimes n}$. These should not be confused with the permutations of the photons discussed in Section II A.*

For simplicity, we begin with a special case in which the input state is fully indistinguishable and there are no internal modes. We have

$$\hat{U}|1, \dots, 1\rangle = \hat{U}\hat{P}\hat{P}^\dagger|1, \dots, 1\rangle = \hat{D}\hat{U}|1, \dots, 1\rangle, \quad (\text{A.1})$$

since $|1, \dots, 1\rangle$ is unaffected by permutations of the modes. Then for any s_0, \dots, s_{n-1} , we have

$$\langle s_0 \cdots s_{n-1}|\hat{U}|1, \dots, 1\rangle = \langle s_0 \cdots s_{n-1}|\hat{D}\hat{U}|1, \dots, 1\rangle = d_0^{s_0} \cdots d_{n-1}^{s_{n-1}} \langle s_0 \cdots s_{n-1}|\hat{U}|1, \dots, 1\rangle. \quad (\text{A.2})$$

Since all d_i are nonzero, we conclude that either

$$d^s = 1 \text{ or } \langle s_0 \cdots s_{n-1}|\hat{U}|1, \dots, 1\rangle = 0, \quad (\text{A.3})$$

where $d^s := d_0^{s_0} \cdots d_{n-1}^{s_{n-1}}$. Thus, the output patterns arising with nonzero probability must satisfy $d^s = 1$. These precisely correspond to the known suppression laws for the Fourier and Hadamard cases [17, 21], discussed below.

Note that the only property of $|1, \dots, 1\rangle$ we needed was its invariance under certain permutations of its modes. More generally, suppose that $|\psi\rangle \in \mathcal{H}^{\otimes n}$ is a general pure state of n photons in n external modes, potentially distinguishable. Assume that $P|\psi\rangle = e^{i\phi}|\psi\rangle$. Then the same argument gives

$$\langle s_0 \cdots s_{n-1}|\hat{U}|\psi\rangle = \langle s_0 \cdots s_{n-1}|\hat{U}\hat{P}\hat{P}^\dagger|\psi\rangle = e^{-i\phi} \langle s_0 \cdots s_{n-1}|\hat{D}\hat{U}|\psi\rangle = e^{-i\phi} d^s \langle s_0 \cdots s_{n-1}|\hat{U}|\psi\rangle. \quad (\text{A.4})$$

We conclude that either $d^s = e^{i\phi}$ or $\langle s_0 \cdots s_{n-1}|\hat{U}|\psi\rangle = 0$. We summarize in the following lemma.

Lemma A.2. [18] *Let U , P , and D be $n \times n$ unitary matrices, with P a permutation matrix and D diagonal with diagonal entries d_0, \dots, d_{n-1} . Suppose $UP = DU$. Let $|\psi\rangle$ be a (pure) state of n*

photons in n modes satisfying $\hat{P}|\psi\rangle = e^{i\phi}|\psi\rangle$. If $\langle s_0, \dots, s_{n-1} | \hat{U}|\psi\rangle \neq 0$, we have

$$d_0^{s_0} \dots d_{n-1}^{s_{n-1}} = e^{i\phi}. \quad (\text{A.5})$$

We now apply this result to the calculation of certain transition probabilities. Let

$$\mathcal{S} = \{|s_0, \dots, s_{n-1}\rangle : \sum s_j = n, d^s = 1\} \quad (\text{A.6})$$

be the set of output patterns arising with nonzero probability from P -symmetric input. We decompose the state space into eigenspaces for P with eigenvalues $e^{i\phi}$. For any $|\psi'\rangle$ with eigenvalue $e^{i\phi} \neq 1$ and $|s\rangle \in \mathcal{S}$, the lemma implies $\langle s | \hat{U}|\psi'\rangle = 0$. Then, for arbitrary $|\eta\rangle$, decompose

$$|\eta\rangle = \langle \eta_+ | \eta \rangle |\eta_+\rangle + |\eta_\perp\rangle, \quad (\text{A.7})$$

where $|\eta_+\rangle$ is the unit vector projection of $|\eta\rangle$ into the +1-eigenspace and $|\eta_\perp\rangle$ collects the terms from other eigenspaces. We have, for $|s\rangle \in \mathcal{S}$,

$$\langle s | \hat{U}|\eta\rangle = \langle s | \hat{U}(\langle \eta_+ | \eta \rangle |\eta_+\rangle + |\eta_\perp\rangle) = \langle \eta_+ | \eta \rangle \langle s | \hat{U}|\eta_+\rangle. \quad (\text{A.8})$$

More generally, consider an abelian group G of $n \times n$ permutation matrices, where each $P \in G$ has corresponding diagonal matrix D_P with $UP = D_P U$. Let $d_{P,i}$ index the diagonal entries of D_P , with d_P^s extending the d^s notation above. We consider the set of output patterns that occur with nonzero probability for all $P \in G$:

$$\mathcal{S}_G = \{|s\rangle : \forall P \in G, d_P^s = 1\}. \quad (\text{A.9})$$

We may generalize the above argument to obtain the following, Part 1 of Theorem III.10:

Lemma A.3. *Let all notation be as above. Let $|\eta\rangle$ be an arbitrary pure state, and let $|\eta_+\rangle$ be its projection into the joint +1-eigenspace of all $P \in G$, normalized to be a unit vector (if nonzero). For $|s\rangle \in \mathcal{S}_G$, we have*

$$\langle s | \hat{U}|\eta\rangle = \langle \eta_+ | \eta \rangle \langle s | \hat{U}|\eta_+\rangle. \quad (\text{A.10})$$

Further, if $|s\rangle \notin \mathcal{S}_G$ and $\langle \eta_+ | \eta \rangle \neq 0$, then $\langle s | \hat{U}|\eta\rangle = 0$.

Proof. Since G is abelian, we may decompose $\mathcal{H}^{\otimes n}$ into a direct sum of joint eigenspaces for G . We index these eigenspaces V_α by functions $\alpha : G \rightarrow \mathbb{C}^*$, such that for $P \in G$ and $|\eta_\alpha\rangle \in V_\alpha$, we have

$$P|\eta_\alpha\rangle = \alpha(P)|\eta_\alpha\rangle. \quad (\text{A.11})$$

Note that if $\alpha \neq \beta$, then V_α is orthogonal to V_β . In particular, given $|\eta\rangle$ as above, we may

decompose

$$|\eta\rangle = \sum_{\alpha} c_{\alpha} |\eta_{\alpha}\rangle, \quad (\text{A.12})$$

where the set of all nonzero $|\eta_{\alpha}\rangle$ is an orthonormal set and $c_{\alpha} = \langle \eta_{\alpha} | \eta \rangle$. The term $|\eta_{+}\rangle$ above corresponds to α trivial, $\alpha(P) = 1$ for all $P \in G$. Now consider $|s\rangle \in \mathcal{S}_G$, so that all $d_P^s = 1$. If α is nontrivial, find P such that $\alpha(P) \neq 1$. We have $d_P^s = 1 \neq \alpha(P)$, so by Lemma A.2, $\langle s | \hat{U} | \eta_{\alpha} \rangle = 0$. This gives the first claim; the second is a direct consequence of Lemma A.2. \square

In other words, to calculate the output probabilities of patterns in \mathcal{S}_G , it suffices to consider the projection of $|\eta\rangle$ into the space of G -symmetric vectors. Since $|1, \dots, 1\rangle$ is fully symmetric, we observe the following:

Lemma A.4. *Let all notation be as above. Let $|s\rangle$ satisfy $\langle s | \hat{U} | 1, \dots, 1 \rangle \neq 0$. Then $|s\rangle \in \mathcal{S}_G$.*

In particular, the *ideal patterns* discussed in Section III A satisfy $|s\rangle = |s_0, \dots, s_{n-1}\rangle$, with $s_0 = 1$ and $\langle s | \hat{U} | 1, \dots, 1 \rangle \neq 0$. Then the ideal patterns are a subset of \mathcal{S}_G ; to calculate $\langle s | \hat{U} | \eta \rangle$ for an ideal pattern $|s\rangle$, it suffices to consider $\langle s | \hat{U} | \eta_{+} \rangle$.

For later use, we consider a special case. Assume that for all $P \in G$, we have $\langle \eta | P | \eta \rangle \in \{0, 1\}$, so that each permutation either fixes $|\eta\rangle$ or takes it to an orthogonal state. Let K be the *stabilizer* of $|\eta\rangle$, the subgroup of G with $P | \eta \rangle = | \eta \rangle$ for $P \in K$. Letting G/K be the set of left cosets of K in G , we have

$$|\eta_{+}\rangle = \frac{1}{\sqrt{|G/K|}} \sum_{g \in G/K} g | \eta \rangle. \quad (\text{A.13})$$

Note that

$$\langle \eta_{+} | \eta \rangle = \frac{1}{\sqrt{|G/K|}} = \sqrt{|K|/|G|} \geq \frac{1}{\sqrt{|G|}}. \quad (\text{A.14})$$

2. Fourier case

As an important example, we consider the Fourier case, $U = F_n$. We use the notation $\omega = e^{2\pi i/n}$. Take the permutation matrix P to correspond to the cyclic permutation $(12 \cdots n)$. We get $UP = DU$, where $d_i = \omega^i$. The group G of symmetries is the cyclic group generated by P . Then the set $\mathcal{S} = \mathcal{S}_G$ consists of $|s_0, \dots, s_{n-1}\rangle$ with

$$1 = \prod_i \omega^{is_i} = \omega^{\sum_i is_i}, \quad (\text{A.15})$$

or equivalently $\sum_i is_i \equiv 0 \pmod{n}$. This is the Zero Transmission Law (ZTL) for the Fourier transform [21]. We call the patterns in \mathcal{S} *ZTL patterns*. This is typically rephrased as in Section III A above, by letting g_0, \dots, g_{n-1} be the weakly decreasing sequence for which s_i counts the number of j with $g_j = i$. The ZTL then translates to $\sum_i gi \equiv 0 \pmod{n}$.

By Lemma A.4, the ideal patterns must be a subset of \mathcal{S} . However, as discussed in Section III A above, there exist ZTL patterns $|s\rangle$ with $s_0 = 1$ that are *not* ideal patterns. (This is discussed in the original paper [21] without the $s_0 = 1$ restriction.) In other words, these patterns satisfy the required symmetry conditions but still cannot be obtained from the input state $|1, \dots, 1\rangle$. Conjecturally, this seems to occur when n is not a prime power. (As shown in the following section, when n is a prime power, the ZTL patterns exactly characterize the ideal patterns.) The first example arises for $n = 6$, where there are 6 ZTL patterns $|s\rangle$ with $s_0 = 1$ that are not ideal patterns. These are:

$$(1, 0, 1, 1, 2, 1), (1, 0, 2, 0, 1, 2), (1, 1, 0, 1, 1, 2), (1, 1, 2, 1, 1, 0), (1, 2, 1, 0, 2, 0), (1, 2, 1, 1, 0, 1). \quad (\text{A.16})$$

a. *Fourier case for prime powers*

In this section, we prove the following theorem:

Theorem A.5. *Let $n = p^r$, where p is a prime. Let g_0, \dots, g_{n-1} be a list of integers in $0, \dots, n-1$ satisfying $\sum_i g_i \equiv 0 \pmod{n}$. Let A be the $n \times n$ matrix whose i th row is the g_i th row of F_n . Then $\text{perm}(A) \neq 0$. In particular, for the corresponding Fock basis state $|s\rangle$ satisfying the Zero Transmission Law, we have $\langle s|U|1, \dots, 1\rangle \neq 0$.*

The second statement follows from the first, by the permanent formulation of boson sampling [32]. By adding the restriction $s_0 = 1$, we immediately obtain

Corollary A.6. *Let $n = p^r$, where p is a prime. Then for the distillation protocol corresponding to $U = F_n$, all ZTL patterns are ideal patterns.*

We now prove the first statement of Theorem A.5. We will very closely follow the argument of [17] for the Hadamard case, substituting a result of [33] at a key point.

Proof. Let A be as above. We use the Laplace expansion of the permanent,

$$\text{perm}(A) = \sum_{j=0}^{n-1} a_{0j} \text{perm}(M_{0j}), \quad (\text{A.17})$$

where a_{ij} is the (i, j) entry of A and M_{ij} is the corresponding minor. We note that we choose $i = 0$ arbitrarily here, and this choice does not affect the proof.

For any $0 \leq \ell \leq n-1$, let A_ℓ be the matrix with the 0th row of A replaced by the ℓ th row of U . In particular, $A_{g_0} = A$. For $\ell \neq g_0$, we have $\ell + g_1 + \dots + g_{n-1} \not\equiv 0 \pmod{n}$, so by the Zero Transmission Law [18, 21] we have $\text{perm}(A_\ell) = 0$.

Letting \vec{u}_i be (the transpose of) the i th row of U and \vec{c} be the vector with entries $\text{perm}(M_{00})$, $\text{perm}(M_{01})$, \dots , $\text{perm}(M_{0(n-1)})$, we have

$$\text{perm}(A_\ell) = \vec{u}_\ell \cdot \vec{c}, \quad (\text{A.18})$$

which vanishes for $\ell \neq g_0$. Since the rows of U must be an orthonormal basis for \mathbb{C}^n , if we can show $\vec{c} \neq 0$ then we may conclude $\text{perm}(A) = \vec{u}_{g_0} \cdot \vec{c} \neq 0$.

To prove that $\vec{c} \neq 0$, we refer to Theorem 2 of [33], which proves that if $n = p^r$ is a prime power, all $(n-1) \times (n-1)$ matrices with entries in the p th roots of unity have nonzero permanent. In our setting, $\sqrt{n}F_n$ has entries in the p th roots of unity, and thus its minors satisfy the assumptions of [33]. We conclude that all entries of \vec{c} are nonzero (a stronger statement than required), and therefore $\text{perm}(A)$ is nonzero. \square

Then the Zero Transmission Law exactly characterizes the ideal patterns when n is a prime power. When n is not a prime power, the above argument fails only in the final step: the analogue of [33] Theorem 2 does not hold for arbitrary n , so it is possible for the vector \vec{c} to be zero. In particular, for any pattern $|s\rangle$ satisfying the ZTL but with $\langle s|U|1, \dots, 1\rangle = 0$, we must have n not a prime power and *all* of the $(n-1) \times (n-1)$ minors of A must have permanent 0.

3. Hadamard case

We now consider the Hadamard case. We let $n = 2^r$ and identify $\mathcal{H}_{\text{ext}} = \mathbb{C}^n$ with $(\mathbb{C}^2)^{\otimes n}$ by representing kets by binary strings. We take $U = H_n = H^{\otimes r}$, where H is the 2×2 Hadamard matrix. Let X and Z be the 2×2 Pauli matrices. Of course, H satisfies $HX = ZH$. This is, in fact, a special case of the framework above, since X is a permutation matrix and Z is diagonal. Following (A.6), we find that in the case $n = 2$, \mathcal{S} consists of patterns $|s_0, s_1\rangle$ with $s_0 + s_1 = 2$ and $(-1)^{s_1} = 1$. In other words, $s_0, s_1 \in \{0, 2\}$, recovering the classic Hong-Ou-Mandel effect.

We may extend this analysis to obtain symmetries of H_n by taking tensor products. We consider the following symmetry group G of U :

$$G = \{X^{i_1} \otimes X^{i_2} \otimes \dots \otimes X^{i_r} : i_j \in \{0, 1\}\}. \quad (\text{A.19})$$

These satisfy

$$H_n(X^{i_1} \otimes X^{i_2} \otimes \dots \otimes X^{i_r}) = (Z^{i_1} \otimes \dots \otimes Z^{i_r})H_n. \quad (\text{A.20})$$

We will compute S_G , defined as above. Letting X_i and Z_i be the actions of X and Z on the i th tensor factor, we note that G is generated by X_1, \dots, X_r and $H_n X_i = Z_i H_n$. To proceed, we will write down the map $\mathbb{H}_{\text{ext}} = \mathbb{C}^n \rightarrow (\mathbb{C}^2)^{\otimes n}$ explicitly: for $k = \sum_{j=0}^{n-1} c_j 2^j$, we map $|k\rangle \mapsto |c_0, \dots, c_{n-1}\rangle$. Then $Z_i |k\rangle = (-1)^{c_i} |k\rangle$. We now consider what the X_i symmetry tells us about $|s\rangle = |s_0, \dots, s_n\rangle \in \mathcal{H}_{\text{ext}}^{\otimes n}$. As discussed in Section III A, we convert to "first quantization," letting g_0, \dots, g_{n-1} be the weakly increasing sequence with s_0 copies of 0, s_1 copies of 1, etc. The g_j can be viewed as the list of modes occupied by the n photons. Let $(g_j)_i$ be the coefficient of 2^i in the binary expansion of s_j . By Lemma A.2, we see that $|s\rangle \in S_G$ only if $\sum_j (g_j)_i \equiv 0 \pmod{2}$. (In other words, $(g_0)_i \oplus \dots \oplus (g_{n-1})_i = 0$, where \oplus represents the XOR of two bits.) Since we may consider symmetries arising from all X_i , this must hold for all i . Then we recover the characterization of

\mathcal{S}_G discussed in [17] and Section III A above: extending \oplus to represent the bitwise XOR operation, $|s\rangle \in \mathcal{S}_G$ if and only if $g_0 \oplus \dots \oplus g_{n-1} = 0$.

Unlike the case of the Fourier transform, in the Hadamard case the symmetries given fully characterize the ideal patterns. In other words, the ideal patterns for $U = H_n$ are the elements of \mathcal{S}_G with $s_0 = 1$. (This is proven in [17] without the additional condition $s_0 = 1$.)

Appendix B: Detailed calculations

Here we discuss the calculations for heralding probabilities and error rates in detail. Let U be the n -mode Fourier or Hadamard matrix, with corresponding symmetry group G . Consider the URS model with parameter R , or the limiting OBB model. Recall the decomposition (II.15) of the n -photon state with error rate ϵ :

$$\rho^{(n)}(\epsilon) = \sum_{k=0}^n \binom{n}{k} \epsilon^k (1-\epsilon)^{n-k} \Phi_k, \quad (\text{B.1})$$

where Φ_k is the (normalized) uniform mixture of all states

$$a_0^\dagger[\xi_{j_0}] \dots a_{n-1}^\dagger[\xi_{j_{n-1}}] |\vec{0}\rangle = |1, \dots, 1\rangle_{2Q} \otimes |\xi_{j_0}, \dots, \xi_{j_{n-1}}\rangle \quad (\text{B.2})$$

(recalling (II.14)) with k distinguishability errors, meaning that k of the indices j_0, \dots, j_{n-1} are nonzero. For example, in the $R = 1$ (SBB) case, Φ_k has $\binom{n}{k}$ terms, corresponding to a choice of k distinguishable photons. For general R , Φ_k has $\binom{n}{k} k^R$ terms; first we choose the k distinguishable photons, then each one has R choices of internal state. In the OBB limit, since each photon has a unique error state, Φ_k again has $\binom{n}{k}$ terms to consider, corresponding to a choice of k distinguishable photons.

In the following subsections, we will consider detailed computations with the heralding and error rates, of both theoretical and computational importance. For practical purposes, we will see that in order to calculate these rates as an *exact* function of ϵ , one must only compute, for all $|\eta\rangle$ of the form (B.2), $h_n(|\eta\rangle\langle\eta|)$ and $e_n(|\eta\rangle\langle\eta|)$.

1. Heralding rate

First we discuss the heralding rate. As discussed in Section III B, we can calculate the heralding rate via

$$h_n(\epsilon) = \sum_{k=0}^n \binom{n}{k} \epsilon^k (1-\epsilon)^{n-k} h_n(\Phi_k). \quad (\text{B.3})$$

Since Φ_k is a uniform mixture, $h_n(\Phi_k)$ is simply the average heralding rate for states of the form (B.2) with k distinguishability errors.

As observed in Lemma A.4, the ideal patterns are a subset of those in \mathcal{S}_G with $s_0 = 1$. By

Lemma A.3, then, we have

$$h_n(|\eta\rangle\langle\eta|) = \sum_{|s\rangle \text{ ideal}} \left| \langle s | \hat{U} |\eta\rangle \right|^2 = |\langle \eta_+ | \eta \rangle|^2 \sum_{|s\rangle \text{ ideal}} \left| \langle s | \hat{U} |\eta_+\rangle \right|^2 = h_n(|\eta_+\rangle\langle\eta_+|). \quad (\text{B.4})$$

This gives the heralding rate statement in Part 2 of Theorem III.10. To prove the corresponding statement in Part 3, we consider the sum over ideal patterns. In the Hadamard case, the ideal patterns are exactly characterized by the conditions $|s\rangle \in \mathcal{S}_G$, $s_0 = 1$. In the Fourier case, this no longer holds in general, although in many cases, the patterns satisfying $\langle s | \hat{U} |\eta\rangle \neq 0$ and $s_0 = 1$ are guaranteed to be ideal. This includes when $|\eta\rangle$ has 0 or 1 distinguishability errors, as in Appendix B3 below. This also holds when n is a prime power, as proven in Appendix A2a. (Also see the discussion of Remark III.11.) Thus, going forward, we will assume that for all patterns $|s\rangle \in \mathcal{S}_G$ with $s_0 = 1$ and $\langle s | \hat{U} |\eta\rangle \neq 0$, we have $|s\rangle$ ideal. Then from this assumption and Lemma A.2, we may include extra vanishing terms to extend the sum to all $|s\rangle$ with $s_0 = 1$:

$$h_n(|\eta\rangle\langle\eta|) = |\langle \eta_+ | \eta \rangle|^2 \sum_{|s\rangle: s_0=1} \left| \langle s | \hat{U} |\eta_+\rangle \right|^2 \quad (\text{B.5})$$

$$= |\langle \eta_+ | \eta \rangle|^2 \left| \langle (|1\rangle \otimes I) \hat{U} |\eta_+\rangle \right|^2 \quad (\text{B.6})$$

$$= |\langle \eta_+ | \eta \rangle|^2 \langle \eta_+ | \hat{U}^\dagger (|1\rangle\langle 1| \otimes I) \hat{U} |\eta_+\rangle. \quad (\text{B.7})$$

This allows for the computation of heralding probabilities without needing to check for ideal patterns. This gives the heralding rate statement in Part 3 of Theorem III.10.

We may further simplify as follows. We have $\langle 1 | = \langle \vec{0} | a_0$, where $a_0 = \sum_i a_0[\xi_i]$ is the external annihilation operator (which is summed over all ξ_i so that it annihilates photons regardless of distinguishability). Then $|1\rangle\langle 1| \otimes I = a_0^\dagger (|0\rangle\langle 0| \otimes I) a_0$. Since the entries in the first row of U are uniformly equal to $1/\sqrt{n}$, we have

$$\hat{U}^\dagger a_0^\dagger = \frac{1}{\sqrt{n}} \sum_i a_i^\dagger \hat{U}^\dagger \quad (\text{B.8})$$

and thus

$$h_n(|\eta\rangle\langle\eta|) = \frac{1}{n} |\langle \eta_+ | \eta \rangle|^2 \sum_{i,j} \langle \eta_+ | a_i^\dagger \hat{U}^\dagger (|0\rangle\langle 0| \otimes I) \hat{U} a_j |\eta_+\rangle. \quad (\text{B.9})$$

We note that $\hat{U}^\dagger (|0\rangle\langle 0| \otimes I) \hat{U}$ is a product of three operators, each of which acts in a “linear optical” way, transforming each photon independently (and all acting only on external modes). For \hat{U} , \hat{U}^\dagger this is by definition; meanwhile, $|0\rangle\langle 0| \otimes I$ acts on each creation operator by $a_i^\dagger \mapsto \delta_{i \neq 0} a_i^\dagger$. Then the product has the same linear optical form. By the unitarity of U and (again) the fact that the entries in its first row are uniformly equal to $1/\sqrt{n}$, we may write

$$\hat{U}^\dagger (|0\rangle\langle 0| \otimes I) \hat{U} = \hat{\Pi}, \quad (\text{B.10})$$

recalling the notation \hat{T} for an operator (not necessarily unitary) acting independently on each photon, as introduced in Section II A. Here, the operator Π on \mathcal{H} is defined by $\Pi = I - \frac{1}{n}\mathbf{1}$, where $\mathbf{1}$ satisfies $\mathbf{1}a_i^\dagger = \left(\sum_{j=0}^{n-1} a_j^\dagger\right)\mathbf{1}$. In particular, $\frac{1}{n}\mathbf{1}$ is the projection into the mode-symmetric subspace of \mathcal{H} , and Π is the complementary projection. We have

$$h_n(|\eta\rangle\langle\eta|) = \frac{1}{n}|\langle\eta_+|\eta\rangle|^2 \sum_{i,j} \langle\eta_+| a_i^\dagger \hat{\Pi} a_j |\eta_+\rangle. \quad (\text{B.11})$$

a. Ideal heralding

We now compute $h_n(0)$ by considering the special case of (B.11) with $|\eta\rangle = |\eta_+\rangle = |1, \dots, 1\rangle_{2Q}$, a perfectly indistinguishable Fock state. More generally, these results apply to any pure tensor of $|1, \dots, 1\rangle_{2Q}$ with an internal state. This will be used in Appendix B 3 below. We also note that the above assumptions involving the relationship between ideal and symmetry-preserving patterns are not needed here. In fact, we will only assume that U is an $n \times n$ unitary matrix with all entries in its first row equal to $1/\sqrt{n}$. By definition, the ideal patterns are those with $s_0 = 1$ and $\langle s|\hat{U}|\eta\rangle \neq 0$, so we may immediately express the heralding rate in the form (B.7), then simplify as above to obtain (B.11).

Now, we write

$$a_j |1, \dots, 1\rangle = \prod_{r \neq j} a_r^\dagger |\vec{0}\rangle. \quad (\text{B.12})$$

Applying $\hat{\Pi}$, we obtain

$$a_j |1, \dots, 1\rangle = \prod_{r \neq j} \left(a_r^\dagger - \frac{1}{n} \sum_v a_v^\dagger \right) |\vec{0}\rangle. \quad (\text{B.13})$$

Then the heralding rate becomes

$$h_n(0) = \frac{1}{n} \sum_{i,j} \langle \vec{0} | \prod_{r' \neq i} a_{r'} \prod_{r \neq j} \left(a_r^\dagger - \frac{1}{n} \sum_v a_v^\dagger \right) |\vec{0}\rangle. \quad (\text{B.14})$$

We note that the terms in this sum are invariant up to relabeling of the modes. Then each term may be reduced to one of two cases, $i = j = 0$ or $i = 1, j = 0$. The former occurs n times and the latter $n^2 - n = n(n - 1)$ times. We obtain

$$h_n(0) = \langle \vec{0} | \prod_{r' \neq 0} a_{r'} \prod_{r \neq 0} \left(a_r^\dagger - \frac{1}{n} \sum_v a_v^\dagger \right) |\vec{0}\rangle \quad (\text{B.15})$$

$$+ (n - 1) \langle \vec{0} | \prod_{r' \neq 1} a_{r'} \prod_{r \neq 0} \left(a_r^\dagger - \frac{1}{n} \sum_v a_v^\dagger \right) |\vec{0}\rangle. \quad (\text{B.16})$$

Labeling the terms in (B.15) and (B.16) as B_n and L_n respectively, we have

Lemma B.1.

$$B_n = \left(\frac{-1}{n}\right)^{n-1} (n-1)! \sum_{t=0}^{n-1} \frac{(-n)^t}{t!} \quad (\text{B.17})$$

$$L_n = \left(\frac{-1}{n}\right)^{n-1} (n-1)! \sum_{t=0}^{n-1} (n-t-1) \frac{(-n)^t}{t!}. \quad (\text{B.18})$$

Note that the lemma immediately gives

$$h_n(0) = B_n + L_n = \left(\frac{-1}{n}\right)^{n-1} (n-1)! \sum_{t=0}^{n-1} (n-t) \frac{(-n)^t}{t!}, \quad (\text{B.19})$$

which proves Theorem III.4. In the remainder of this section, we will prove the lemma, which is a straightforward counting argument. We focus on B_n , with L_n being similar.

We view B_n as the inner product of $a_1^\dagger \cdots a_{n-1}^\dagger |\vec{0}\rangle$ and $\prod_{r>0} \left(a_r^\dagger - \frac{1}{n} \sum_v a_v^\dagger\right) |\vec{0}\rangle$. In particular, we expand the latter and sum the coefficients involving exactly one $a_{r'}^\dagger$ for all $r' > 0$ (and no a_0^\dagger). Each term in the expansion is a product of some number t of the a_r^\dagger and $n-1-t$ other a_v^\dagger chosen from some $\frac{1}{n} \sum_v a_v^\dagger$. These terms vanish in the inner product unless the a_r^\dagger all have $r > 0$ and the a_v^\dagger involve the remaining $n-1-t$ nonzero indices. Then we expand as follows, where t is the number of a_r^\dagger used, as above, and c_t is the number of such nonvanishing terms:

$$B_n = \langle \vec{0} | a_1 \cdots a_{n-1} \prod_{r>0} \left(a_r^\dagger - \frac{1}{n} \sum_v a_v^\dagger\right) |\vec{0}\rangle \quad (\text{B.20})$$

$$= \langle \vec{0} | a_1 \cdots a_{n-1} \sum_{t=0}^{n-1} \left(\frac{-1}{n}\right)^{n-1-t} c_t a_1^\dagger \cdots a_{n-1}^\dagger |\vec{0}\rangle \quad (\text{B.21})$$

$$= \sum_{t=0}^{n-1} \left(\frac{-1}{n}\right)^{n-1-t} c_t. \quad (\text{B.22})$$

We note there are $\binom{n-1}{t}$ ways to choose t distinct values of a_r^\dagger , then $(n-1-t)!$ ways to choose which factors the remaining a_v^\dagger come from. This gives

$$c_t = \left(\frac{-1}{n}\right)^{n-1-t} \binom{n-1}{t} (n-1-t)! = \left(\frac{-1}{n}\right)^{n-1-t} \frac{(n-1)!}{t!} = \left(\frac{-1}{n}\right)^{n-1} (n-1)! \frac{(-n)^t}{t!}, \quad (\text{B.23})$$

proving the result for B_n .

b. Ideal heralding asymptotics

We now prove Theorem III.4 Part 2 giving the asymptotic formula for $h_n(0)$, following the proof of Kotesovec. We let $W(z)$ be the Lambert W function, the principal branch of the multi-valued solution to the equation $W(z)e^{W(z)} = z$.

First, by Theorem III.4 Part 1, we have

$$n^{n-1}h_n(0) = (-1)^{n-1}(n-1)! \sum_{t=0}^{n-1} (n-t) \frac{(-n)^t}{t!}. \quad (\text{B.24})$$

For $n \geq 1$, elementary algebraic manipulation recovers the formula for the exponential generating function of $-1/(1 - W(-z))$ given on the OEIS [25]. In other words, expanding

$$\frac{-1}{1 - W(-z)} = \sum_{n \geq 0} w_n z^n, \quad (\text{B.25})$$

we have

$$h_n(0) = \frac{n!}{n^{n-1}} w_n. \quad (\text{B.26})$$

By Stirling's formula, this gives

$$h_n(0) \sim \frac{\sqrt{2\pi n^{3/2}}}{e^n} w_n. \quad (\text{B.27})$$

Now, following Kotesovec, we use the Maple library *gdev*. Specifically, we use the procedure *equivalent*, which applies saddle point methods to determine the asymptotic behavior of coefficients of generating functions [26]. From the command

$$\text{equivalent}(-1/(1 - \text{LambertW}(-z)), z, n, 1), \quad (\text{B.28})$$

we find

$$w_n \sim \frac{e^n}{4\sqrt{2\pi n^{3/2}}}. \quad (\text{B.29})$$

Then by (B.27),

$$h_n(0) \sim \frac{\sqrt{2\pi n^{3/2}}}{e^n} \cdot \frac{e^n}{4\sqrt{2\pi n^{3/2}}} = \frac{1}{4}, \quad (\text{B.30})$$

giving Theorem III.4 Part 2.

2. Error rate

We now discuss the calculation of error rates. The error rate is a conditional probability: the probability that the output photon is distinguishable, given successful heralding. In our setting, this is calculated as follows. First (extending notation to arbitrary input states as usual), we may write the conditional probability $e_n(\rho)$ as a quotient of $\bar{e}_n(\rho)$, the probability of successful heralding *and* distinguishable output, divided by $h_n(\rho)$, the probability of successful heralding. In particular,

we have

$$e_n(\epsilon) = \frac{\bar{e}_n(\epsilon)}{h_n(\epsilon)}. \quad (\text{B.31})$$

The denominator may be calculated as in Appendix B1, so we focus on $\bar{e}_n(\epsilon)$ here. As with the other notation, we extend the notation \bar{e}_n to arbitrary input states and write

$$\bar{e}_n(\epsilon) = \sum_{k=1}^n \binom{n}{k} \epsilon^k (1-\epsilon)^{n-k} \bar{e}_n(\Phi_k) \quad (\text{B.32})$$

(noting that $\bar{e}_n(\Phi_0) = 0$). Of course, $\bar{e}_n(\Phi_k)$ is the average of $\bar{e}_n(|\eta\rangle\langle\eta|)$ over all $|\eta\rangle$ of the form (B.2) with k distinguishability errors. Let $|\eta\rangle$ be such a term. To calculate $\bar{e}_n(|\eta\rangle\langle\eta|)$, we perform an internal-external measurement on $\hat{U}|\eta\rangle$; that is, we project onto the desymmetrized Fock states and calculate the probability that the external state is ideal and the photon in the output mode 0 has internal state ξ_i , $i > 0$.

As above, by Lemma A.3 (or rather, its slight extension to internal-external measurements) we may write

$$\bar{e}_n(|\eta\rangle\langle\eta|) = |\langle\eta_+|\eta\rangle|^2 \bar{e}_n(|\eta_+\rangle\langle\eta_+|). \quad (\text{B.33})$$

Dividing both sides by $h_n(|\eta\rangle\langle\eta|)$, applying (B.4), and rewriting $\bar{e}_n(\rho) = e_n(\rho)h_n(\rho)$, we obtain

$$e_n(|\eta\rangle\langle\eta|) = e_n(|\eta_+\rangle\langle\eta_+|). \quad (\text{B.34})$$

This completes Part 2 of Theorem III.10.

Similarly to the heralding rate, we may rewrite the expression for $\bar{e}_n(|\eta\rangle\langle\eta|)$ in a way that removes the burden of checking that the output pattern satisfies the appropriate symmetries:

$$\bar{e}_n(|\eta\rangle\langle\eta|) = |\langle\eta_+|\eta\rangle|^2 \sum_{i \geq 1} |(\langle 0| \otimes I) a_0[\xi_i] \hat{U} |\eta_+\rangle|^2. \quad (\text{B.35})$$

This requires the assumption that the relevant patterns in \mathcal{S}_G are ideal, as discussed in Remark III.11 and Appendix B1. This completes the proof of Part 3 of Theorem III.10.

Again writing $\bar{e}_n(\Phi_k) = e_n(\Phi_k)h_n(\Phi_k)$, we note that we have the following expression for the error rate:

$$e_n(\epsilon) = \frac{\sum_{k=1}^n \binom{n}{k} \epsilon^k (1-\epsilon)^{n-k} e_n(\Phi_k) h_n(\Phi_k)}{\sum_{k=0}^n \binom{n}{k} \epsilon^k (1-\epsilon)^{n-k} h_n(\Phi_k)} = \frac{\sum_{k=1}^n \binom{n}{k} \epsilon^k (1-\epsilon)^{n-k} e_n(\Phi_k) \tilde{h}_n(\Phi_k)}{1 + \sum_{k=1}^n \binom{n}{k} \epsilon^k (1-\epsilon)^{n-k} \tilde{h}_n(\Phi_k)}, \quad (\text{B.36})$$

where $\tilde{h}_n(\Phi_k) = h_n(\Phi_k)/h_n(\Phi_0)$. These expressions $\tilde{h}_n(\Phi_k)$ are given conjectured bounds in Conjecture III.12. Thus the error rate can be described in terms of these relatively well understood ratios of heralding rates and the quantities $e_n(\Phi_k)$.

3. First order approximations

We now return to the setting of the URS (or OBB) model of photon distinguishability. We assume that ϵ is independent of n and consider approximations of $h_n(\epsilon)$ and $e_n(\epsilon)$ up to first order in ϵ . As discussed in Section III B, we have

$$h_n(\epsilon) = h_n(0) + \epsilon n(h_n(\Phi_1) - h_n(0)) + O(\epsilon^2), \quad (\text{B.37})$$

where Φ_1 is the evenly weighted probabilistic mixture of all terms of the form (II.14) involving exactly one distinguishability error. Further, from (B.31) and (B.32), we see that

$$e_n(\epsilon) = \epsilon n e_n(\Phi_1) + O(\epsilon^2). \quad (\text{B.38})$$

Then the first-order approximations require only knowledge of $h_n(0)$, discussed above, and $h_n(\Phi_1)$, $e_n(\Phi_1)$. Further, we will find that all terms of Φ_1 exhibit the same behavior with regard to distillation protocols. Without loss of generality, we will consider

$$|\eta\rangle = a_0^\dagger[\xi_1] a_1^\dagger[\xi_0] \cdots a_{n-1}^\dagger[\xi_0] |\vec{0}\rangle. \quad (\text{B.39})$$

We will consider $U = F_n$ or $U = H_n$. Note that we will *not* place any additional assumptions on the relationship between ideal patterns and those in \mathcal{S}_G , so we allow all $n = 2^r$ in the Hadamard case and all $n \geq 3$ in the Fourier case. In either context, we have an abelian symmetry group G of order n , and all $P|\eta\rangle$ are mutually orthogonal for $P \in G$. Explicitly, these permutations correspond to permuting the single “distinguishable” photon to each of the modes $0, \dots, n-1$. By the discussion in Section A 1, we obtain the associated G -symmetrization

$$|\eta_+\rangle = \frac{1}{\sqrt{n}} \sum_{i=0}^{n-1} a_0^\dagger[\xi_0] \cdots a_{i-1}^\dagger[\xi_0] a_i^\dagger[\xi_1] a_{i+1}^\dagger[\xi_0] \cdots a_{n-1}^\dagger[\xi_0] |\vec{0}\rangle, \quad \text{with } \langle \eta_+ | \eta \rangle = \frac{1}{\sqrt{n}}. \quad (\text{B.40})$$

We note that $|\eta_+\rangle$ is invariant under *arbitrary* permutations of the external modes, not just those in G . In fact, by direct computation we see that

$$|\eta_+\rangle = \text{symm} \left(|0, 1, \dots, n-1\rangle_{1Q} \right) \otimes \text{symm} (|\xi_1, \xi_0, \dots, \xi_0\rangle) \quad (\text{B.41})$$

$$= |1, \dots, 1\rangle_{2Q} \otimes (|\xi_1, \xi_0, \dots, \xi_0\rangle + |\xi_0, \xi_1, \xi_0, \dots, \xi_0\rangle + \cdots + |\xi_0, \dots, \xi_0, \xi_1\rangle). \quad (\text{B.42})$$

In other words, $|\eta_+\rangle$ is a perfectly indistinguishable state, a pure tensor of the Fock state $|1, \dots, 1\rangle_{2Q}$ and some symmetric internal state. Then the results of Appendix B 1 a apply here, and we have

$$h_n(|\eta\rangle\langle\eta|) = \frac{1}{n} h_n(|\eta_+\rangle\langle\eta_+|) = \frac{1}{n} h_n(0). \quad (\text{B.43})$$

Further, since all terms of Φ_1 have the same symmetrization (up to relabeling of the $|\xi_i\rangle$, $i > 0$),

we have

$$h_n(\Phi_1) = \frac{1}{n} h_n(0). \quad (\text{B.44})$$

This gives Theorem III.3.

Next we consider the output error rate. In this setting, we may characterize $e_n(|\eta_+\rangle\langle\eta_+|)$ as the probability that, given successful heralding of a single output photon, the output photon has internal state $|\xi_1\rangle$. Since $|\eta_+\rangle$ is a pure tensor as described above, and linear optics and PNRD only act on the external part of the state, the post-heralding state is still a pure tensor with the same internal part given in (B.41). This internal part is fully symmetric, so the probability of any given photon having internal state $|\xi_1\rangle$ is exactly $1/n$. Then by (B.34),

$$e_n(\Phi_1) = e_n(|\eta_+\rangle\langle\eta_+|) = \frac{1}{n}. \quad (\text{B.45})$$

This proves Theorem III.2.

Appendix C: Haar random case

For comparison with the distillation schemes outlined in the main text and how they utilize interference to assist in distilling errors, we provide analysis in the case where random unitaries are considered for distillation. Interestingly, although these unitaries have no special structure, they can still be used for distillation purposes. However, as we will see, the protocols based around random matrices are significantly less resource efficient than the Fourier protocol of the main text. This highlights the importance of the specific constructive and destructive interference in the latter scheme.

We consider generating Haar random unitaries from $U(n)$ (where the number of photons, n , is the same as the number of modes) and, as a warm up, running the same distillation protocols as outlined in this work. In particular, we evolve the all 1 state $|\bar{1}\rangle = |1, \dots, 1\rangle$ under a sampled random matrix, compute the ideal heralding patterns that have exactly 1 photon out in mode 0 (which as the matrix is random, it will typically include all possible patterns), and study how the heralding probabilities scale. By concentration of measure [34], for large enough n we expect a typical sample to be well described by the average, and so we can use Haar averaging to compute quantities of interest.

First we can ask what the heralding rate $h_n(0)$ is. This is the probability that a single photon exits in mode 0, from the initial all 1 state. We compute this as follows:

$$h_n(0) = \int d\mu_{\hat{U}} \langle \bar{1} | \hat{U}^\dagger (|1\rangle\langle 1| \otimes \mathbf{I}_{n-1, n-1}) \hat{U} | \bar{1} \rangle. \quad (\text{C.1})$$

That is, the state $|\bar{1}\rangle$ is evolved under unitary \hat{U} , we compute the probability of PNRD giving an output pattern with a single photon in mode 0, then we average over all unitaries. Note that here, the \hat{U} are $d_{n,n} \times d_{n,n}$ matrices, where $d_{n,m}$ is the dimension of the space of n photons in m modes

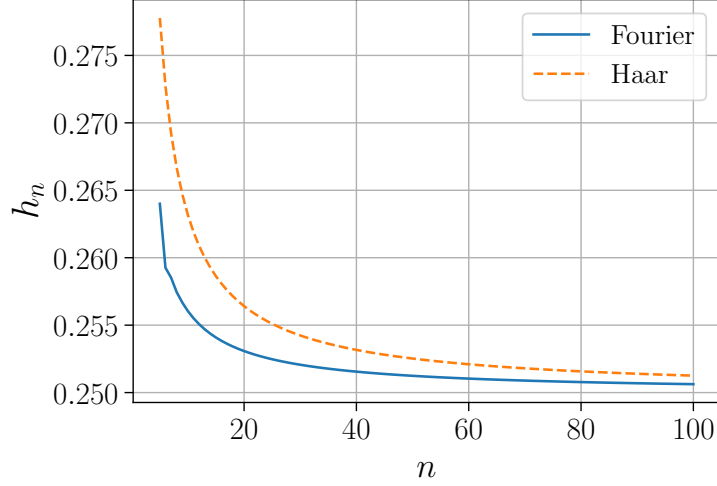


FIG. 13: Haar and Fourier distillation schemes heralding rate at 0 error ($h_n(0)$), as a function of n (i.e., the probability a single photon exits from mode 0, in the absence of error).

$[d_{n,m} = \binom{n+m-1}{n}]$. The identity matrix $\mathbf{I}_{n-1,n-1}$ on $n-1$ modes and $n-1$ photons has dimension $d_{n-1,n-1}$.

Whilst the underlying linear optical unitary is drawn from a Haar random distribution on $U(n)$, it does not imply the $d_{n,n} \times d_{n,n}$ matrices \hat{U} are Haar random in $U(d_{n,n})$. However, as shown in Ref. [24], linear optical unitaries are a 1-design. As such, we can still treat the integral in the above equation as a Haar random integral ($\int d\mu_U U X U^\dagger = \text{Tr}[X] \mathbb{I}/d$), which we can analytically evaluate as:

$$h_n(0) = \frac{\text{Tr}[\mathbf{I}_{n-1,n-1}]}{d_{n,n}} = \frac{d_{n-1,n-1}}{d_{n,n}} = \frac{1}{4} \frac{1}{1 - (2n)^{-1}} > 1/4. \quad (\text{C.2})$$

Of course this makes intuitive sense; for a random unitary, one expects any particular state is equally likely with probability $1/d_{n,n}$ (when averaged over unitaries), and the total number of states with 1 photon in mode 0 is $d_{n-1,n-1}$. Notice that as with Theorem III.4 and Conjecture III.6 (pertaining to the Fourier and Hadamard matrices), this is decreasing monotonically in n and tends to $1/4$. We additionally conjecture that Eq. (C.2) is an upper bound for the same sized protocol with the Fourier matrices. See Fig. 13 for some numerics.

We can further calculate what happens at first order errors (where there are $n-1$ identical photons, and 1 in an orthogonal internal state). Now there are four integrals similar to Eq. (C.1); we care about getting 1 or 0 photons out starting with $n-1$ identical photons in n modes, and conversely 0 or 1 photons out starting with 1 (error) photon. Multiplying these as written gives respectively the probability of observing an ideal photon out of the scheme, or an error photon, in the case of exactly one error. These can be computed in the same manner as Eq. (C.1), and combining the results gives two probabilities:

$$P_{ideal} = \frac{d_{n-2,n-1}}{d_{n-1,n}} \frac{d_{1,n-1}}{d_{1,n}} = \frac{1}{4} \frac{(1 - 1/n)^2}{1 - \frac{3}{2n}}, \quad P_{err} = \frac{d_{n-1,n-1}}{d_{n-1,n}} \frac{d_{0,n-1}}{d_{1,n}} = \frac{1}{2n}. \quad (\text{C.3})$$

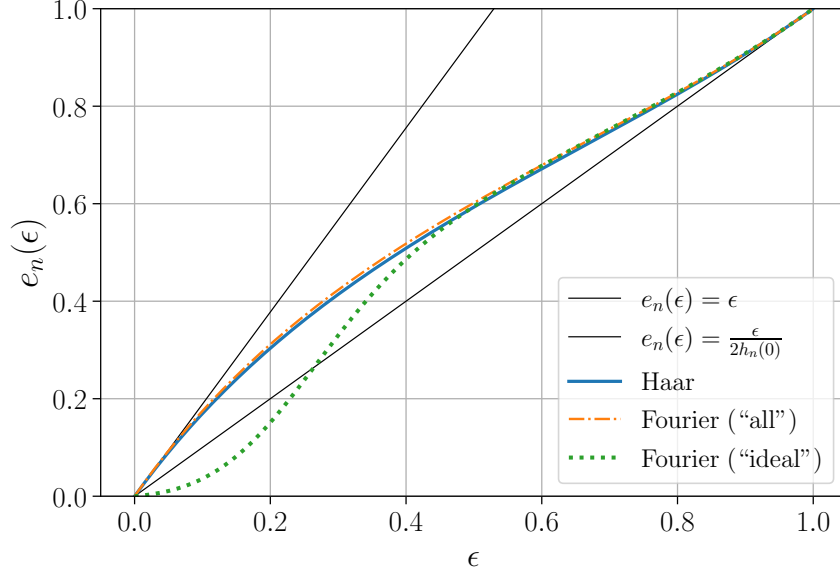


FIG. 14: ‘Distillation’ from a single instance drawn from the Haar random distribution for $n = 9$, with the OBB error model, where we post-select on all possible patterns (solid blue line). Distillation is useful when $e_n(\epsilon) < \epsilon$ (lower solid black line), which is never the case here. For small $\epsilon \lesssim 0.1$ we see it follows the upper solid line, Eq. (C.4). For comparison, we also include the case where we post-select on the ideal patterns in the Fourier protocol at $n = 9$ (dotted line), which we see for $\epsilon \lesssim 0.25$ results in $e_n(\epsilon) < \epsilon$. If we run the Fourier protocol but allow one to post-select on all valid patterns (dash-dot), the scaling is similar to the Haar case.

The first term corresponds to the probability an ideal photon exits mode 0, and the second term the probability the error (distinguishable) photon exits mode 0, given exactly 1 distinguishability error at the input.

We can compute the output fidelity of the scheme at first order using $h_n(0), P_{ideal}, P_{err}$:

$$f_n(\epsilon) := 1 - e_n(\epsilon) \approx \frac{h_n(0)(1 - \epsilon)^n + n\epsilon(1 - \epsilon)^{n-1}P_{ideal}}{h_n(0)(1 - \epsilon)^n + n\epsilon(1 - \epsilon)^{n-1}(P_{ideal} + P_{err})} \approx 1 - \frac{\epsilon}{2h_n(0)}. \quad (\text{C.4})$$

Since $h_n(0) < 0.5$ for $n \geq 3$, we see the output error $e_n(\epsilon) \approx \epsilon/2h_n(0)$ has actually *increased*, and for large enough n , $e_n(\epsilon) \approx 2\epsilon$. We verify this scaling numerically in Fig. 14. Note that we numerically obtain similar scaling $e_n(\epsilon) \approx 2\epsilon$ in the Fourier case if we post-select on all possible outcomes with 1 output photon, as opposed to only ideal patterns (see Fig. 14). Therefore, this result is more about the fact that we are post-selecting on all possible patterns, not necessarily related to interference or lack thereof in the Haar vs. Fourier case.

A more interesting comparison is where we take a particular (random) unitary, and use only the highest weight heralding patterns resulting from the evolution of the initial all 1 state (such that there is 1 photon out in mode 0). The intuition here is that from a (single instance of a) Haar random unitary in $U(n)$, the probabilities will be Porter-Thomas distributed (by the 1-design property of \hat{U}). As such, there will be a set of patterns that will have a relatively high weight (i.e.,

above the mean probability, $1/d_{n,n}$), distributed according to de^{-dp} , where p is the probability and $d = d_{n,n}$ (the expected number of states with probability greater than p^* is $\approx de^{-dp^*}$). The high weight patterns undergo a degree of constructive interference, akin to the patterns used for Fourier/Hadamard distillation. As such, one may expect these patterns could be used for photon distillation, despite the underlying unitary being random.

We provide numerics for this protocol in Fig. 15, which shows that if one post-selects on only the several highest-weighted patterns for that particular unitary, up to around 30% of the total weight, distillation does work (i.e. it reduces the error, when the initial error ϵ is small). However, as can also be seen in the figure (right), the heralding probability decreases as we reduce the number of post-selection patterns and thus the error $\tilde{e}_n(\epsilon)$ (we put ‘tilde’ above to differentiate this from the protocols of the main text). This is in contrast to the Fourier protocol in the main text, where at low error, the heralding probability is close to 1/4 for all n , while the error reduces by a factor of n . Moreover, here the error reduction factor at small error seems to be at most by a factor of ≈ 2 (i.e., at small ϵ , $\tilde{e}_n(\epsilon) \approx \epsilon/2$). Again, we can contrast this to the Fourier protocol, which has $e_n(\epsilon) \approx \epsilon/n$.

We can provide some analytics on this protocol too. First, consider the case where one uses only the highest weight pattern for post-selection (this corresponds to the x-axis at 0 in Fig. 15). As the probabilities are Porter-Thomas distributed, the largest expected probability is $p^* = \frac{1}{d} \log d$ (i.e., the expected number of states with probability greater than p^* is 1). However, since the fraction of states that have 1 photon out in mode 0 is $d_{n-1,n-1}/d_{n,n}$ (see Eq. (C.2)) we need to solve instead the following equation:

$$N_{p>p^*} = d_{n,n}e^{-d_{n,n}p^*} = \frac{d_{n,n}}{d_{n-1,n-1}} \implies p^* = \frac{1}{d_{n,n}} \log d_{n-1,n-1} \quad (\text{C.5})$$

This is the expected probability of the highest weight state with 1 photon out in mode 0. Whilst the distillation scheme that selects only the highest weighted pattern has the greatest error reduction, the heralding probability decreases with the dimension.

If instead we select the highest weighted k patterns (with 1 photon out in mode 0), by similar reasoning as above, the cumulative probability is:

$$\tilde{h}_n^{(k)}(0) = \frac{1}{d_{n,n}} \sum_{i=1}^k \log \frac{d_{n-1,n-1}}{i} = \frac{1}{d_{n,n}} (k \log d_{n-1,n-1} - \log k!) \approx r \frac{d_{n-1,n-1}}{d_{n,n}} (1 - \log r). \quad (\text{C.6})$$

For the fraction of all possible patterns $r = k/d_{n-1,n-1}$ “large enough”, the equation can be re-written via Stirling’s approximation as on the right hand side. For $r \rightarrow 1$ this reproduces $\tilde{h}_n^{(k)} \approx \frac{d_{n-1,n-1}}{d_{n,n}}$ as expected from Eq. (C.2) ($r = 1$ is equivalent to post-selecting on all possible patterns). We show how the analytic function compares to data for $n = 7$ in Fig. 16.

This analysis shows that distillation is not a unique phenomena, in fact, it is typically possible for an arbitrary unitary, so long as there are a subset of patterns that have relatively high constructive interference. However, distillation from random unitaries is generally much more expensive (compared to say the Fourier protocol) as shown in Fig. 15 and the subsequent analysis

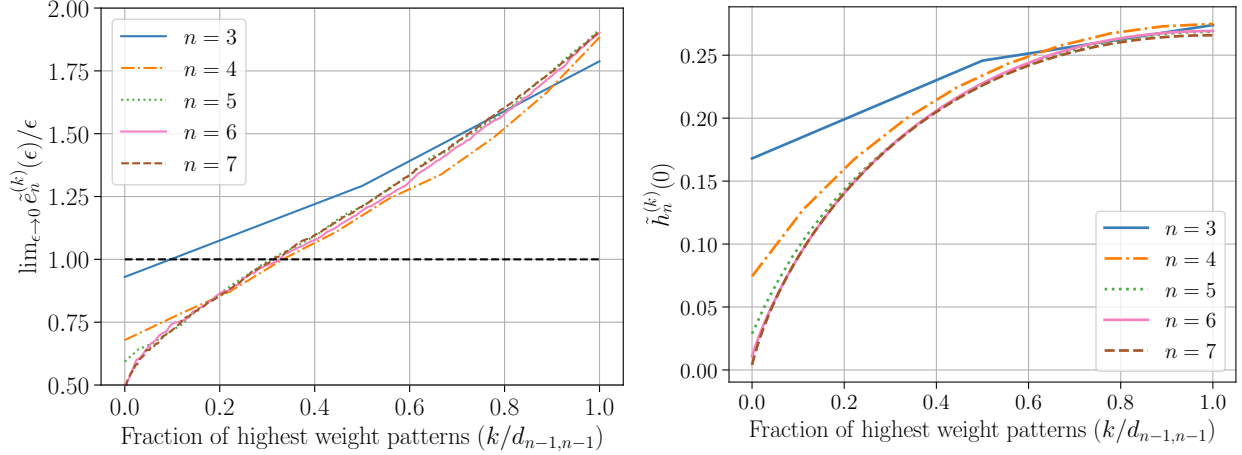


FIG. 15: Distillation using Haar random unitaries, where post-selection is on a fraction of the highest weight (probability) output patterns (i.e., if one enumerated all states, those with the most constructive interference would be positioned towards the left on the x-axis). To show the data for different n on a consistent axis, $x = 0$ corresponds to including the single highest weight pattern, and $x = 1$ to including all patterns. Each curve is an average of at least 100 Haar random unitaries. Left: Error reduction relative to the initial error ϵ , at ‘small’ ϵ . We see for $n = 4, 5, 6, 7$, there is a distillation effect when the top $\lesssim 30\%$ of the highest weight patterns are used. As expected from Eq. (C.4), this tends to $\bar{e}_n(\epsilon)/\epsilon \approx 2$ when all patterns are used. Right: Heralding rate at 0 error for the protocol that selects a certain percentage of the highest weight patterns. As expected from Eq. (C.2) it tends to a little over $1/4$, when using all possible patterns.

above; the heralding rates are lower and the error is reduced by a lesser amount. The nature of the constructive interference in the Fourier (and Hadamard) unitaries is what allows for an efficient protocol, where the weight concentrates on a relatively small subset of all possible patterns, as per the zero-transmission laws, ultimately as a result of symmetry in the matrices (Sect. A 1).

Appendix D: Numerics

Here we list the functions for the heralding rate $h_n(\epsilon)$ and $\bar{e}_n(\epsilon) := h_n(\epsilon)e_n(\epsilon)$, where the coefficients are given up to 6 decimal places. The superscript denotes Hadamard (H) or Fourier (F) protocol, along with the error model (SBB or OBB). We go up to protocols of size $n = 16$.

$$h_3^{(F,OBB)}(\epsilon) = -0.444444\epsilon^3 + 1.0\epsilon^2 - 0.666667\epsilon + 0.333333$$

$$g_3^{(F,OBB)}(\epsilon) = -0.111111\epsilon^3 + 0.222222\epsilon^2 + 0.111111\epsilon$$

$$h_4^{(F,OBB)}(\epsilon) = 0.21875\epsilon^4 - 0.875\epsilon^3 + 1.25\epsilon^2 - 0.75\epsilon + 0.25$$

$$g_4^{(F,OBB)}(\epsilon) = 0.0625\epsilon^4 - 0.15625\epsilon^3 + 0.125\epsilon^2 + 0.0625\epsilon$$

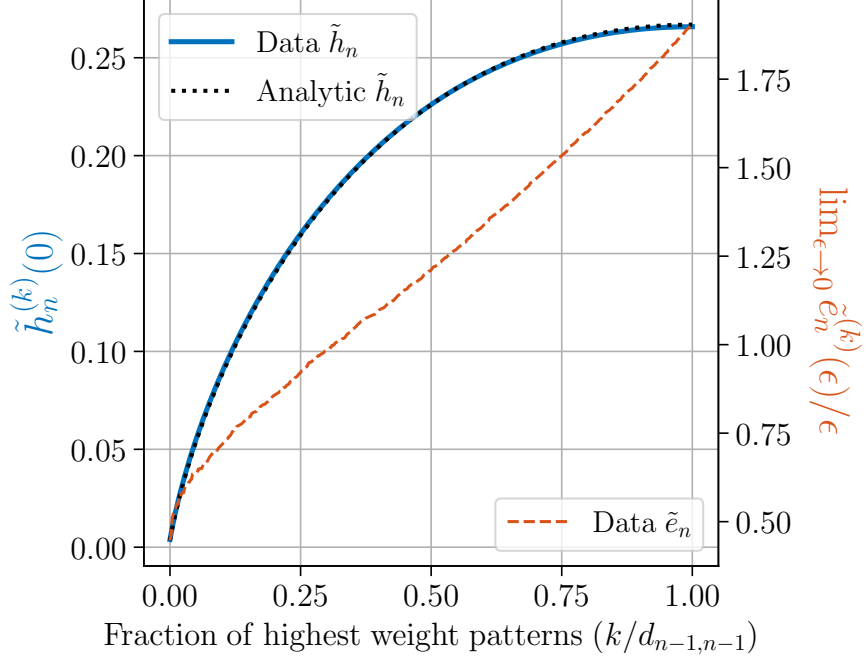


FIG. 16: The same data as in Fig. 15 for the $n = 7$ case, with the analytically computed heralding rate, Eq. (C.6) (dotted line). The dashed line (red) pertains to the right y-axis.

$$h_5^{(F, OBB)}(\epsilon) = -0.3008\epsilon^5 + 1.352\epsilon^4 - 2.496\epsilon^3 + 2.32\epsilon^2 - 1.056\epsilon + 0.264$$

$$g_5^{(F, OBB)}(\epsilon) = -0.0752\epsilon^5 + 0.2752\epsilon^4 - 0.3552\epsilon^3 + 0.1856\epsilon^2 + 0.0528\epsilon$$

$$h_6^{(F, OBB)}(\epsilon) = 0.164095\epsilon^6 - 1.074074\epsilon^5 + 2.861111\epsilon^4 - 3.990741\epsilon^3 + 3.104938\epsilon^2 - 1.296296\epsilon + 0.259259$$

$$g_6^{(F, OBB)}(\epsilon) = -0.001029\epsilon^6 - 0.03035\epsilon^5 + 0.130658\epsilon^4 - 0.151235\epsilon^3 + 0.037037\epsilon^2 + 0.04321\epsilon$$

$$h_7^{(F, OBB)}(\epsilon) = -0.269276\epsilon^7 + 1.819658\epsilon^6 - 5.300649\epsilon^5 + 8.5891\epsilon^4 - 8.355923\epsilon^3 + 4.866365\epsilon^2$$

$$- 1.551139\epsilon + 0.258523$$

$$g_7^{(F, OBB)}(\epsilon) = -0.045534\epsilon^7 + 0.264431\epsilon^6 - 0.635781\epsilon^5 + 0.819284\epsilon^4 - 0.581008\epsilon^3 + 0.198336\epsilon^2$$

$$+ 0.036932\epsilon$$

$$h_8^{(F, OBB)}(\epsilon) = 0.254355\epsilon^8 - 2.013817\epsilon^7 + 6.954575\epsilon^6 - 13.711838\epsilon^5 + 16.879898\epsilon^4 - 13.285034\epsilon^3$$

$$+ 6.515625\epsilon^2 - 1.802124\epsilon + 0.257446$$

$$g_8^{(F, OBB)}(\epsilon) = 0.028242\epsilon^8 - 0.201295\epsilon^7 + 0.61639\epsilon^6 - 1.045336\epsilon^5 + 1.064926\epsilon^4 - 0.63929\epsilon^3$$

$$+ 0.193268\epsilon^2 + 0.032181\epsilon$$

$$\begin{aligned}
h_9^{(F, OBB)}(\epsilon) &= -0.259805\epsilon^9 + 2.30374\epsilon^8 - 9.085128\epsilon^7 + 20.897056\epsilon^6 - 30.898198\epsilon^5 + 30.452286\epsilon^4 \\
&\quad - 20.003042\epsilon^3 + 8.433139\epsilon^2 - 2.053421\epsilon + 0.256678 \\
g_9^{(F, OBB)}(\epsilon) &= -0.031193\epsilon^9 + 0.248405\epsilon^8 - 0.863248\epsilon^7 + 1.712829\epsilon^6 - 2.119439\epsilon^5 + 1.676531\epsilon^4 \\
&\quad - 0.816684\epsilon^3 + 0.207585\epsilon^2 + 0.02852\epsilon
\end{aligned}$$

$$\begin{aligned}
h_{10}^{(F, OBB)}(\epsilon) &= 0.224292\epsilon^{10} - 2.248157\epsilon^9 + 10.131033\epsilon^8 - 27.050042\epsilon^7 + 47.415965\epsilon^6 - 57.048908\epsilon^5 \\
&\quad + 47.727882\epsilon^4 - 27.421711\epsilon^3 + 10.349609\epsilon^2 - 2.304346\epsilon + 0.256038 \\
g_{10}^{(F, OBB)}(\epsilon) &= 0.015023\epsilon^{10} - 0.141072\epsilon^9 + 0.580919\epsilon^8 - 1.374501\epsilon^7 + 2.067219\epsilon^6 - 2.058328\epsilon^5 \\
&\quad + 1.362179\epsilon^4 - 0.569992\epsilon^3 + 0.124606\epsilon^2 + 0.025604\epsilon
\end{aligned}$$

$$\begin{aligned}
h_{11}^{(F, OBB)}(\epsilon) &= -0.258321\epsilon^{11} + 2.812722\epsilon^{10} - 13.924191\epsilon^9 + 41.361968\epsilon^8 - 81.918457\epsilon^7 + 113.577362\epsilon^6 \\
&\quad - 112.48887\epsilon^5 + 79.58329\epsilon^4 - 39.410684\epsilon^3 + 12.999835\epsilon^2 - 2.555117\epsilon + 0.255512 \\
g_{11}^{(F, OBB)}(\epsilon) &= -0.026051\epsilon^{11} + 0.257516\epsilon^{10} - 1.145395\epsilon^9 + 3.019497\epsilon^8 - 5.224039\epsilon^7 + 6.198709\epsilon^6 \\
&\quad - 5.107336\epsilon^5 + 2.885973\epsilon^4 - 1.061283\epsilon^3 + 0.214231\epsilon^2 + 0.023228\epsilon
\end{aligned}$$

$$\begin{aligned}
h_{12}^{(F, OBB)}(\epsilon) &= 0.209933\epsilon^{12} - 2.517528\epsilon^{11} + 13.880187\epsilon^{10} - 46.484937\epsilon^9 + 105.269933\epsilon^8 - 169.791286\epsilon^7 \\
&\quad + 199.995617\epsilon^6 - 173.357903\epsilon^5 + 109.775093\epsilon^4 - 49.535757\epsilon^3 + 15.122094\epsilon^2 \\
&\quad - 2.805752\epsilon + 0.255068 \\
g_{12}^{(F, OBB)}(\epsilon) &= 0.012932\epsilon^{12} - 0.131845\epsilon^{11} + 0.627022\epsilon^{10} - 1.819979\epsilon^9 + 3.557862\epsilon^8 - 4.89237\epsilon^7 \\
&\quad + 4.808945\epsilon^6 - 3.361442\epsilon^5 + 1.625987\epsilon^4 - 0.501301\epsilon^3 + 0.067693\epsilon^2 \\
&\quad + 0.021256\epsilon
\end{aligned}$$

$$\begin{aligned}
h_{13}^{(F, OBB)}(\epsilon) &= -0.256575\epsilon^{13} + 3.312358\epsilon^{12} - 19.737578\epsilon^{11} + 71.876417\epsilon^{10} - 178.469408\epsilon^9 + 319.071887\epsilon^8 \\
&\quad - 422.566319\epsilon^7 + 419.736502\epsilon^6 - 312.705065\epsilon^5 + 172.571856\epsilon^4 - 68.568569\epsilon^3 \\
&\quad + 18.565529\epsilon^2 - 3.056287\epsilon + 0.254691 \\
g_{13}^{(F, OBB)}(\epsilon) &= -0.021507\epsilon^{13} + 0.256063\epsilon^{12} - 1.397339\epsilon^{11} + 4.621636\epsilon^{10} - 10.318372\epsilon^9 + 16.382755\epsilon^8 \\
&\quad - 18.967277\epsilon^7 + 16.134565\epsilon^6 - 10.007414\epsilon^5 + 4.413923\epsilon^4 - 1.306331\epsilon^3 \\
&\quad + 0.219146\epsilon^2 + 0.019592\epsilon
\end{aligned}$$

$$\begin{aligned}
h_{14}^{(F, OBB)}(\epsilon) &= 0.248631\epsilon^{14} - 3.468923\epsilon^{13} + 22.467367\epsilon^{12} - 89.537764\epsilon^{11} + 245.30117\epsilon^{10} \\
&\quad - 488.735103\epsilon^9 + 730.308668\epsilon^8 - 831.480622\epsilon^7 + 724.836377\epsilon^6 \\
&\quad - 481.471758\epsilon^5 + 239.895246\epsilon^4 - 86.943662\epsilon^3 + 21.659326\epsilon^2 \\
&\quad - 3.306744\epsilon + 0.254365 \\
g_{14}^{(F, OBB)}(\epsilon) &= 0.015783\epsilon^{14} - 0.207283\epsilon^{13} + 1.254585\epsilon^{12} - 4.633648\epsilon^{11} + 11.654902\epsilon^{10} \\
&\quad - 21.087845\epsilon^9 + 28.242459\epsilon^8 - 28.349749\epsilon^7 + 21.330084\epsilon^6 \\
&\quad - 11.879343\epsilon^5 + 4.759748\epsilon^4 - 1.292818\epsilon^3 + 0.201532\epsilon^2 \\
&\quad + 0.018169\epsilon
\end{aligned}$$

$$\begin{aligned}
h_{15}^{(F, OBB)}(\epsilon) &= -0.241853\epsilon^{15} + 3.616164\epsilon^{14} - 25.241632\epsilon^{13} + 109.101123\epsilon^{12} - 326.544436\epsilon^{11} \\
&\quad + 716.893158\epsilon^{10} - 1192.598009\epsilon^9 + 1530.879003\epsilon^8 - 1528.868594\epsilon^7 \\
&\quad + 1187.961675\epsilon^6 - 712.369085\epsilon^5 + 323.77471\epsilon^4 - 107.975136\epsilon^3 \\
&\quad + 24.937876\epsilon^2 - 3.557138\epsilon + 0.254081 \\
g_{15}^{(F, OBB)}(\epsilon) &= -0.016062\epsilon^{15} + 0.221733\epsilon^{14} - 1.426197\epsilon^{13} + 5.654597\epsilon^{12} - 15.425275\epsilon^{11} \\
&\quad + 30.607378\epsilon^{10} - 45.534487\epsilon^9 + 51.578136\epsilon^8 - 44.688305\epsilon^7 \\
&\quad + 29.463423\epsilon^6 - 14.544347\epsilon^5 + 5.210035\epsilon^4 - 1.27289\epsilon^3 \\
&\quad + 0.177233\epsilon^2 + 0.016939\epsilon
\end{aligned}$$

$$\begin{aligned}
h_{16}^{(F, OBB)}(\epsilon) &= 0.253335\epsilon^{16} - 4.038754\epsilon^{15} + 30.18027\epsilon^{14} - 140.322429\epsilon^{13} + 454.349967\epsilon^{12} \\
&\quad - 1086.337589\epsilon^{11} + 1984.048773\epsilon^{10} - 2823.471777\epsilon^9 + 3164.084293\epsilon^8 \\
&\quad - 2801.498604\epsilon^7 + 1953.285982\epsilon^6 - 1061.16792\epsilon^5 + 440.365482\epsilon^4 \\
&\quad - 134.9397\epsilon^3 + 28.786057\epsilon^2 - 3.807482\epsilon + 0.253832 \\
g_{16}^{(F, OBB)}(\epsilon) &= 0.014883\epsilon^{16} - 0.224239\epsilon^{15} + 1.576554\epsilon^{14} - 6.861315\epsilon^{13} + 20.672222\epsilon^{12} \\
&\quad - 45.672554\epsilon^{11} + 76.443663\epsilon^{10} - 98.700638\epsilon^9 + 99.11872\epsilon^8 \\
&\quad - 77.419864\epsilon^7 + 46.65063\epsilon^6 - 21.295698\epsilon^5 + 7.128947\epsilon^4 \\
&\quad - 1.645702\epsilon^3 + 0.222265\epsilon^2 + 0.015865\epsilon
\end{aligned}$$

$$\begin{aligned}
h_3^{(F, SBB)}(\epsilon) &= 0.666667\epsilon^2 - 0.666667\epsilon + 0.333333 \\
g_3^{(F, SBB)}(\epsilon) &= 0.222222\epsilon^3 + 0.111111\epsilon
\end{aligned}$$

$$h_4^{(F,SBB)}(\epsilon) = 0.5\epsilon^4 - 1.0\epsilon^3 + 1.25\epsilon^2 - 0.75\epsilon + 0.25$$

$$g_4^{(F,SBB)}(\epsilon) = 0.25\epsilon^4 - 0.125\epsilon^3 + 0.0625\epsilon^2 + 0.0625\epsilon$$

$$h_5^{(F,SBB)}(\epsilon) = 1.12\epsilon^4 - 2.24\epsilon^3 + 2.176\epsilon^2 - 1.056\epsilon + 0.264$$

$$g_5^{(F,SBB)}(\epsilon) = 0.1984\epsilon^5 + 0.064\epsilon^4 - 0.0896\epsilon^3 + 0.0384\epsilon^2 + 0.0528\epsilon$$

$$h_6^{(F,SBB)}(\epsilon) = 0.469136\epsilon^6 - 1.407407\epsilon^5 + 3.320988\epsilon^4 - 4.296296\epsilon^3 + 3.209877\epsilon^2 - 1.296296\epsilon + 0.259259$$

$$g_6^{(F,SBB)}(\epsilon) = 0.234568\epsilon^6 - 0.17284\epsilon^5 + 0.333333\epsilon^4 - 0.222222\epsilon^3 + 0.04321\epsilon^2 + 0.04321\epsilon$$

$$h_7^{(F,SBB)}(\epsilon) = 1.653954\epsilon^6 - 4.961861\epsilon^5 + 8.179806\epsilon^4 - 8.089844\epsilon^3 + 4.769084\epsilon^2 - 1.551139\epsilon + 0.258523$$

$$g_7^{(F,SBB)}(\epsilon) = 0.203538\epsilon^7 + 0.114595\epsilon^6 - 0.304618\epsilon^5 + 0.430076\epsilon^4 - 0.31441\epsilon^3 + 0.09241\epsilon^2$$

$$+ 0.036932\epsilon$$

$$h_8^{(F,SBB)}(\epsilon) = 1.196045\epsilon^8 - 4.78418\epsilon^7 + 11.590942\epsilon^6 - 18.028198\epsilon^5 + 19.233032\epsilon^4 - 14.00061\epsilon^3$$

$$+ 6.595093\epsilon^2 - 1.802124\epsilon + 0.257446$$

$$g_8^{(F,SBB)}(\epsilon) = 0.598022\epsilon^8 - 1.458435\epsilon^7 + 2.527679\epsilon^6 - 2.60202\epsilon^5 + 1.755798\epsilon^4 - 0.76062\epsilon^3$$

$$+ 0.164841\epsilon^2 + 0.032181\epsilon$$

$$h_9^{(F,SBB)}(\epsilon) = 1.539102\epsilon^8 - 6.156409\epsilon^7 + 16.150666\epsilon^6 - 26.904567\epsilon^5 + 28.593089\epsilon^4 - 19.527711\epsilon^3$$

$$+ 8.35925\epsilon^2 - 2.053421\epsilon + 0.256678$$

$$g_9^{(F,SBB)}(\epsilon) = 0.173234\epsilon^9 - 0.010003\epsilon^8 + 0.434339\epsilon^7 - 0.58065\epsilon^6 - 0.044621\epsilon^5 + 0.598385\epsilon^4$$

$$- 0.46752\epsilon^3 + 0.124993\epsilon^2 + 0.02852\epsilon$$

$$h_{10}^{(F,SBB)}(\epsilon) = 0.990159\epsilon^{10} - 4.950797\epsilon^9 + 16.84128\epsilon^8 - 37.660339\epsilon^7 + 58.647314\epsilon^6 - 64.924101\epsilon^5$$

$$+ 51.249409\epsilon^4 - 28.327452\epsilon^3 + 10.438872\epsilon^2 - 2.304346\epsilon + 0.256038$$

$$g_{10}^{(F,SBB)}(\epsilon) = 0.49508\epsilon^{10} - 1.283939\epsilon^9 + 3.059071\epsilon^8 - 4.852346\epsilon^7 + 5.42193\epsilon^6 - 4.197144\epsilon^5$$

$$+ 2.206428\epsilon^4 - 0.73143\epsilon^3 + 0.112785\epsilon^2 + 0.025604\epsilon$$

$$\begin{aligned}
h_{11}^{(F,SBB)}(\epsilon) &= 2.673653\epsilon^{10} - 13.368264\epsilon^9 + 39.984461\epsilon^8 - 79.728259\epsilon^7 + 111.228371\epsilon^6 - 110.782916\epsilon^5 \\
&+ 78.750534\epsilon^4 - 39.142649\epsilon^3 + 12.940185\epsilon^2 - 2.555117\epsilon + 0.255512 \\
g_{11}^{(F,SBB)}(\epsilon) &= 0.219724\epsilon^{11} + 0.128347\epsilon^{10} - 0.603985\epsilon^9 + 1.695164\epsilon^8 - 3.128761\epsilon^7 + 3.96735\epsilon^6 \\
&- 3.49346\epsilon^5 + 2.096604\epsilon^4 - 0.795249\epsilon^3 + 0.14655\epsilon^2 + 0.023228\epsilon
\end{aligned}$$

$$\begin{aligned}
h_{12}^{(F,SBB)}(\epsilon) &= 1.631678\epsilon^{12} - 9.790066\epsilon^{11} + 34.093343\epsilon^{10} - 80.724445\epsilon^9 + 145.319173\epsilon^8 - 204.620747\epsilon^7 \\
&+ 223.447065\epsilon^6 - 185.520527\epsilon^5 + 114.357436\epsilon^4 - 50.63467\epsilon^3 + 15.247511\epsilon^2 \\
&- 2.805752\epsilon + 0.255068 \\
g_{12}^{(F,SBB)}(\epsilon) &= 0.815839\epsilon^{12} - 3.468135\epsilon^{11} + 9.198735\epsilon^{10} - 14.830645\epsilon^9 + 16.627012\epsilon^8 - 14.144466\epsilon^7 \\
&+ 9.692648\epsilon^6 - 5.351305\epsilon^5 + 2.230542\epsilon^4 - 0.599913\epsilon^3 + 0.0635\epsilon^2 \\
&+ 0.021256\epsilon
\end{aligned}$$

$$\begin{aligned}
h_{13}^{(F,SBB)}(\epsilon) &= 3.176221\epsilon^{12} - 19.057329\epsilon^{11} + 69.736548\epsilon^{10} - 173.990559\epsilon^9 + 312.479401\epsilon^8 - 415.604865\epsilon^7 \\
&+ 414.448341\epsilon^6 - 309.857728\epsilon^5 + 171.512249\epsilon^4 - 68.301482\epsilon^3 + 18.515491\epsilon^2 \\
&- 3.056287\epsilon + 0.254691 \\
g_{13}^{(F,SBB)}(\epsilon) &= 0.224615\epsilon^{13} + 0.128112\epsilon^{12} - 0.731971\epsilon^{11} + 2.546441\epsilon^{10} - 5.991159\epsilon^9 + 10.044939\epsilon^8 \\
&- 12.307653\epsilon^7 + 11.101794\epsilon^6 - 7.307659\epsilon^5 + 3.407139\epsilon^4 - 1.041312\epsilon^3 \\
&+ 0.161815\epsilon^2 + 0.019592\epsilon
\end{aligned}$$

$$\begin{aligned}
h_{14}^{(F,SBB)}(\epsilon) &= 2.89273\epsilon^{14} - 20.249109\epsilon^{13} + 80.789571\epsilon^{12} - 221.499005\epsilon^{11} + 458.616795\epsilon^{10} \\
&- 745.280196\epsilon^9 + 963.990617\epsilon^8 - 993.4496\epsilon^7 + 809.641849\epsilon^6 \\
&- 514.226497\epsilon^5 + 248.746223\epsilon^4 - 88.426255\epsilon^3 + 21.759622\epsilon^2 \\
&- 3.306744\epsilon + 0.254365 \\
g_{14}^{(F,SBB)}(\epsilon) &= 1.446365\epsilon^{14} - 7.76345\epsilon^{13} + 25.047604\epsilon^{12} - 53.601276\epsilon^{11} + 83.812151\epsilon^{10} \\
&- 100.020547\epsilon^9 + 93.200682\epsilon^8 - 68.615441\epsilon^7 + 39.97736\epsilon^6 \\
&- 18.181655\epsilon^5 + 6.218312\epsilon^4 - 1.469996\epsilon^3 + 0.186087\epsilon^2 \\
&+ 0.018169\epsilon
\end{aligned}$$

$$\begin{aligned}
h_{15}^{(F,SBB)}(\epsilon) &= 1.999291\epsilon^{14} - 13.995039\epsilon^{13} + 69.187563\epsilon^{12} - 233.189868\epsilon^{11} + 562.533669\epsilon^{10} \\
&- 1008.642989\epsilon^9 + 1372.202486\epsilon^8 - 1430.24324\epsilon^7 + 1144.52239\epsilon^6 \\
&- 699.315018\epsilon^5 + 321.289733\epsilon^4 - 107.703994\epsilon^3 + 24.912155\epsilon^2 \\
&- 3.557138\epsilon + 0.254081 \\
g_{15}^{(F,SBB)}(\epsilon) &= 0.148935\epsilon^{15} - 0.117369\epsilon^{14} + 2.101777\epsilon^{13} - 7.610254\epsilon^{12} + 16.626189\epsilon^{11} \\
&- 24.476007\epsilon^{10} + 23.087361\epsilon^9 - 10.667335\epsilon^8 - 3.515025\epsilon^7 \\
&+ 9.700534\epsilon^6 - 7.776713\epsilon^5 + 3.605745\epsilon^4 - 1.005404\epsilon^3 \\
&+ 0.134708\epsilon^2 + 0.016939\epsilon
\end{aligned}$$

$$\begin{aligned}
h_{16}^{(F,SBB)}(\epsilon) &= 6.016855\epsilon^{16} - 48.134837\epsilon^{15} + 204.409141\epsilon^{14} - 588.504346\epsilon^{13} + 1287.423744\epsilon^{12} \\
&- 2264.121037\epsilon^{11} + 3284.378587\epsilon^{10} - 3957.4023\epsilon^9 + 3945.762787\epsilon^8 \\
&- 3224.285091\epsilon^7 + 2129.870547\epsilon^6 - 1116.533163\epsilon^5 + 452.722849\epsilon^4 \\
&- 136.685334\epsilon^3 + 28.889082\epsilon^2 - 3.807482\epsilon + 0.253832 \\
g_{16}^{(F,SBB)}(\epsilon) &= 3.008427\epsilon^{16} - 20.522658\epsilon^{15} + 75.618868\epsilon^{14} - 182.741006\epsilon^{13} + 322.105768\epsilon^{12} \\
&- 437.528923\epsilon^{11} + 472.856403\epsilon^{10} - 413.95135\epsilon^9 + 295.880963\epsilon^8 \\
&- 172.741727\epsilon^7 + 81.809681\epsilon^6 - 30.875009\epsilon^5 + 8.94162\epsilon^4 \\
&- 1.83046\epsilon^3 + 0.20737\epsilon^2 + 0.015865\epsilon
\end{aligned}$$

$$\begin{aligned}
h_4^{(H,OBB)}(\epsilon) &= 0.09375\epsilon^4 - 0.625\epsilon^3 + 1.125\epsilon^2 - 0.75\epsilon + 0.25 \\
g_4^{(H,OBB)}(\epsilon) &= -0.0625\epsilon^4 + 0.09375\epsilon^3 + 0.0625\epsilon
\end{aligned}$$

$$\begin{aligned}
h_8^{(H,OBB)}(\epsilon) &= 0.208449\epsilon^8 - 1.737587\epsilon^7 + 6.259529\epsilon^6 - 12.775833\epsilon^5 + 16.168381\epsilon^4 - 12.995544\epsilon^3 \\
&+ 6.46637\epsilon^2 - 1.802124\epsilon + 0.257446 \\
g_8^{(H,OBB)}(\epsilon) &= -0.029978\epsilon^8 + 0.147674\epsilon^7 - 0.25787\epsilon^6 + 0.126371\epsilon^5 + 0.178909\epsilon^4 - 0.280861\epsilon^3 \\
&+ 0.13266\epsilon^2 + 0.032181\epsilon
\end{aligned}$$

$$\begin{aligned}
h_{16}^{(H,OBB)}(\epsilon) &= 0.230133\epsilon^{16} - 3.71401\epsilon^{15} + 28.069175\epsilon^{14} - 131.873962\epsilon^{13} + 431.097063\epsilon^{12} \\
&- 1039.775789\epsilon^{11} + 1914.096926\epsilon^{10} - 2743.373245\epsilon^9 + 3093.838395\epsilon^8 \\
&- 2754.544589\epsilon^7 + 1929.738735\epsilon^6 - 1052.576617\epsilon^5 + 438.209702\epsilon^4 \\
&- 134.606696\epsilon^3 + 28.762166\epsilon^2 - 3.807482\epsilon + 0.253832 \\
g_{16}^{(H,OBB)}(\epsilon) &= -0.015351\epsilon^{16} + 0.198705\epsilon^{15} - 1.171307\epsilon^{14} + 4.128425\epsilon^{13} - 9.554221\epsilon^{12} \\
&+ 14.808314\epsilon^{11} - 14.347616\epsilon^{10} + 5.172842\epsilon^9 + 8.103302\epsilon^8 \\
&- 16.640031\epsilon^7 + 16.199821\epsilon^6 - 10.197077\epsilon^5 + 4.347022\epsilon^4 \\
&- 1.21646\epsilon^3 + 0.191506\epsilon^2 + 0.015865\epsilon
\end{aligned}$$

$$\begin{aligned}
h_4^{(H,SBB)}(\epsilon) &= 0.75\epsilon^4 - 1.5\epsilon^3 + 1.5\epsilon^2 - 0.75\epsilon + 0.25 \\
g_4^{(H,SBB)}(\epsilon) &= 0.375\epsilon^4 - 0.375\epsilon^3 + 0.1875\epsilon^2 + 0.0625\epsilon
\end{aligned}$$

$$\begin{aligned}
h_8^{(H,SBB)}(\epsilon) &= 4.362183\epsilon^8 - 17.44873\epsilon^7 + 34.335205\epsilon^6 - 41.935059\epsilon^5 + 34.572754\epsilon^4 - 19.610596\epsilon^3 \\
&+ 7.526367\epsilon^2 - 1.802124\epsilon + 0.257446 \\
g_8^{(H,SBB)}(\epsilon) &= 2.181091\epsilon^8 - 7.241394\epsilon^7 + 11.977203\epsilon^6 - 11.803741\epsilon^5 + 7.352905\epsilon^4 - 2.731384\epsilon^3 \\
&+ 0.490585\epsilon^2 + 0.032181\epsilon
\end{aligned}$$

$$\begin{aligned}
h_{16}^{(H,SBB)}(\epsilon) &= 73.066525\epsilon^{16} - 584.532202\epsilon^{15} + 2329.372756\epsilon^{14} - 6076.295754\epsilon^{13} + 11549.027996\epsilon^{12} \\
&- 16898.538369\epsilon^{11} + 19644.483484\epsilon^{10} - 18480.77709\epsilon^9 + 14209.06391\epsilon^8 \\
&- 8957.588849\epsilon^7 + 4617.555313\epsilon^6 - 1928.458556\epsilon^5 + 641.063454\epsilon^4 \\
&- 164.507094\epsilon^3 + 30.871957\epsilon^2 - 3.807482\epsilon + 0.253832 \\
g_{16}^{(H,SBB)}(\epsilon) &= 36.533263\epsilon^{16} - 267.836909\epsilon^{15} + 981.467437\epsilon^{14} - 2349.08095\epsilon^{13} + 4074.399578\epsilon^{12} \\
&- 5394.101741\epsilon^{11} + 5606.674093\epsilon^{10} - 4641.409119\epsilon^9 + 3074.148247\epsilon^8 \\
&- 1622.369985\epsilon^7 + 673.077141\epsilon^6 - 213.838632\epsilon^5 + 49.631079\epsilon^4 \\
&- 7.676514\epsilon^3 + 0.620979\epsilon^2 + 0.015865\epsilon
\end{aligned}$$